

# Deep Node Ranking: an Algorithm for Structural Network Embedding and End-to-End Classification

Blaž Škrlj<sup>1,2</sup>, Jan Kralj<sup>1</sup>, Janez Konc<sup>4</sup>,  
Marko Robnik-Šikonja<sup>5</sup>, and Nada Lavrač<sup>2,3</sup>

<sup>1</sup> Jožef Stefan Institute, Jamova 39, 1000 Ljubljana, Slovenia

<sup>2</sup> Jožef Stefan Int. Postgraduate School, Jamova 39, 1000 Ljubljana, Slovenia

<sup>3</sup> University of Nova Gorica, Vipavska 13, 5000 Nova Gorica, Slovenia

<sup>4</sup> National Institute of Chemistry, Ljubljana, Slovenia

<sup>5</sup> Faculty for computer and information science, Ljubljana, Slovenia  
{blaz.skrlj,nada.lavrac}@ijs.si

**Abstract.** Complex networks are used as an abstraction for systems modeling in physics, biology, sociology, and other areas. We propose an algorithm based on a fast personalized node ranking and recent advancements in deep learning for learning supervised network embeddings as well as to classify network nodes directly. Learning from homogeneous, as well as heterogeneous networks, our algorithm outperforms strong baselines on nine node-classification benchmarks from the domains of molecular biology, finance, social media and language processing—one of the largest node classification collections to date. The results are comparable or better than current state-of-the-art in terms of speed as well as predictive accuracy. Embeddings, obtained by the proposed algorithm, are also a viable option for network visualization.

## 1 Introduction

Many real-world systems consisting of interconnected entities can be represented as complex networks. The study of complex networks offers insights into latent relations between connected entities represented by nodes and has various practical applications, for example discovery of drug targets, modeling of disease outbreaks, author profiling, modeling of transportation, study of social dynamics, etc. [1, 2, 3].

Modern machine learning approaches applied to complex networks offer intriguing opportunities for the development of fast and accurate algorithms that can learn from the topology of a given network. Recently, approaches based on network embedding [4, 5, 6, 7] have become prevalent for many common tasks, such as node classification and edge prediction, as well as for unsupervised clustering. Embedding of a network is a representation of its nodes and edges in a vector space that maintains the topological properties of the network [7]. Embeddings are useful, as vectors are efficient data structures to be used with machine learning algorithms.

Deep neural networks [8, 9] belong to a class of machine learning algorithms in which multiple layers of neurons are stacked on top of each other and trained to predict target classes via backpropagation. Deep learning is widely used in image and text analysis [10], and has only recently been considered for network learning [9, 11] for tasks such as network node classification, (i.e. assigning labels to nodes), and node clustering, where nodes are grouped into clusters according to their shared properties.

In this work, we propose a new network embedding algorithm termed *Deep Node Ranking (DNR)*, which combines efficient personalized node ranking with non-linear approximation power of *deep neural networks*. The developed framework uses deep neural networks to obtain a network embedding directly from stationary node distributions produced by random walkers with restarts. The rationale for development of this approach is that it is currently impossible to analytically derive properties of complex networks, for example node label distributions, that would relate with a network’s topology. We solve this problem using random walk-based network sampling.

Even though there already exist embedding approaches based on higher order random walkers [4], we believe that the stationary distribution of first-order random walkers is unexploited in a deep learning setting. We showcase the developed algorithm on the challenging problems of node classification and network visualization, which highlights the ability of our algorithm to learn and predict meaningful node labels. As test sets for the task of node classification are few, we compile three new data sets from financial and biological domains with distinct network topologies and varying number of target classes. The key contributions of the paper are:

1. A fast, general network embedding algorithm based on global, personalized node ranks, which performs comparably to the state-of-the-art embedding algorithms, and can be used for multitude of downstream learning tasks, such as node classification, network visualization etc.
2. A variation of the above algorithm (1), developed specifically for an *end-to-end* node classification, outperforming embedding approaches, as well as explicit matrix factorization-based approaches.
3. Three novel node classification benchmark data sets from financial and biological domains.

The work is structured as follows. In Section 2, we shortly review related works on learning from complex networks, deep learning, and (personalized) node ranking algorithms. Based on that, we provide a rationale for the development of our approach. Section 3 presents our network node embedding algorithm that combines deep neural networks with network node ranking. In Section 4, we describe the experimental setting and nine different non-synthetic homogeneous complex networks from different domains used in the evaluation. The experimental results are discussed in Section 5. In Section 6 we conclude the work and present ideas for further improvements.

## 2 Background and Related Work

In the following subsections we describe how algorithms learn from complex networks and what is learned, followed by an overview of node ranking algorithms and deep learning preliminaries.

### 2.1 Learning From Complex Networks

Complex networks, representing real-world phenomena, such as financial markets, transportation, biological interactions, or social dynamics [1, 2, 3] often possess interesting properties, such as scale invariance, partitioning, presence of hub nodes, weakly connected components, heavy-tailed node degree distributions, occurrence of communities, significant motif pattern counts etc. [12, 13]. *Learning from complex networks* considers different aspects of complex networks, e.g., network structure and node labels that are used as inputs to machine learning algorithms with the aim to do link prediction, node classification, etc.

Many different approaches to learning from complex networks exist. For example, one of the most common unsupervised approaches, the *community detection* [14], groups the nodes of a network into densely connected sub-networks, and enables learning of hidden properties from complex networks. Communities in complex biological networks correspond to functionally connected biological entities, such as the proteins involved in cancerogenesis. In social networks, communities may correspond to people sharing common interests [15]. Community detection algorithms use random walk-based sampling or graph spectral properties [16, 17, 18] to achieve unsupervised detection of communities within complex networks. In contrast, our methodology focuses on the semi-supervised tasks of *node classification* and *network embedding* described subsequently.

**Node Classification.** Node classification is the problem of classifying nodes in a network into one or many possible labeled classes. It belongs to semi-supervised learning algorithms, as the whole network is used to obtain representations of individual nodes, from which the network classification model is learned. Information propagation algorithms [19] propagate label information via nodes' neighbors until all nodes are labeled. These algorithms learn in an *end-to-end* manner, meaning that no intermediary representation of a network is first obtained and subsequently used as an input for learning.

Another class of node classification algorithms learn node labels from node representations in a vector form (embeddings). Here, the whole network is first transformed into an information-rich low-dimensional representation, for example, a dense matrix (one row for one node). This representation serves as an input to plethora of general machine learning approaches that can be used for node classification.

The proposed DNR algorithm can be viewed as both, the graph embedding approach, and as an end-to-end classification approach (similarly to the

information propagation algorithms). We continue with the discussion of network embedding construction, as it represents the key aspect of the proposed approach.

**Network Embedding.** Network embedding is the process of transforming a given network, its topology as well as node and edge labels, into a learned vector form [20] that can be used in various down-stream (propositional) learning tasks, such as, for example:

- community detection and visualization [14, 6],
- network node and edge classification [4, 7, 5], and
- network alignment and comparison [21].

Many approaches for network embedding have been developed. For example, the LINE algorithm [22] uses the network’s eigendecomposition in order to learn a low dimensional network representation, i.e. a representation of the network in 128 dimensions instead of  $|N|$  (=number of nodes) dimensions. Approaches that use random walks to sample the network include DeepWalk [7] and its generalization node2vec [4]. It was recently proven that DeepWalk, node2vec, and LINE can be reformulated as an implicit matrix factorization [23].

All of the before-mentioned methods aim to preserve topological properties of the input network in the final embedding. There currently exist only a handful of approaches that leverage the deep learning methodology (discussed in Section 2.2) to learn from complex networks directly. One such approach, Structural Deep Network Embedding (SDNE) [11], learns embeddings from the network adjacency matrices generated using deep autoencoders. The authors of this approach have experimentally shown that neural networks with up to three layers suffice for the majority of learning tasks on five different complex networks. When determining the layer sizes and other parameters, they used exhaustive search, which is computationally demanding for such problems.

Despite many promising approaches developed, a recent extensive evaluation of the network embedding techniques [24] suggests that node2vec [4] remains one of the best network embedding approaches for the task of node classification.

## 2.2 Deep Learning Overview

Artificial neural networks were conceptualized in the 1940s, but large scale adoption of deep neural networks was not possible until recently due to their high computational demand [8, 9]. With the advent of scientific computing on graphical processing units (GPUs), deep neural networks emerged as the state-of-the-art approach for learning from complex, structured data sources [10].

Neural network architecture is of paramount importance for achieving successful deep learning [25]. It was empirically demonstrated that a network requires optimization in terms of layer sizes and their connectivity; however, theoretical foundation for network architecture optimization remains an open problem. Various platforms facilitating the construction and evaluation of deep neural networks exist. They include Tensorflow [26], PyTorch [27], Theano [28], and

Caffe [29]. Using these platforms, derivatives used in gradients are computed automatically and hence the user can concentrate on the design and optimization of the network architecture and other aspects of learning.

A deep feedforward neural network consists of an input layer, many hidden layers and an output layer. For two consecutive neural network layers,  $l - 1$  and  $l$ , with  $s_{l-1}$  and  $s_l$  neurons, each layer is a mapping taking as input the output of the previous layer,  $o_{l-1} \in \mathbb{R}^{s_{l-1}}$ , and producing a new output  $o_l \in \mathbb{R}^{s_l}$  as

$$o_l = a(w_l o_{l-1} + b_l) \quad (1)$$

where  $a$  is an activation function,  $w_l \in \mathbb{R}^{s_l \times s_{l-1}}$  is the weight matrix of the layer  $l$ , and  $b_l \in \mathbb{R}^{s_l}$  represents the layer's bias vector. Activation functions introduce non-linearity into the learning process. Some commonly activation functions are the sigmoid, ReLU, and ELU functions, described in detail in the Section 3.2.

During learning, the backpropagation algorithm [30, 31] assigns such weights  $w_l$  and biases  $b_l$  to each layer  $l$  that minimize the distance between the network's output and the desired output, expressed as a cost function. For example, if the input is a set of images and the output is a set of image labels, the backpropagation aims to ensure that the neural network will assign a correct label to each image in the training set. The backpropagation algorithm consists of three repeated steps:

1. The forward pass. The algorithm feeds each training instance to the network and computes the output of every neuron in each consecutive layer. Then it measures the networks output error by evaluating the cost function.
2. The backward pass. The algorithm computes the contribution of each neuron in the last hidden layer to each output neuron's error. The algorithm proceeds to measure how much of these error contributions came from each neuron in the previous hidden layer, and so on until the algorithm reaches the input layer. This backward pass effectively measures the error gradient across all the weights in the network by propagating the error gradient backward in the network.
3. Update of weights and biases. In this step, the algorithm performs a stochastic gradient descent minimization [32] on all the weight matrices and bias vectors of the network using the error gradients measured earlier.

Training feedforward fully connected networks with large multidimensional inputs, such as images or complex networks, may be infeasible due to a huge number of trainable parameters. Convolutional neural networks (CNNs) significantly reduce the number of parameters required by enforcing shared weights and are therefore widely used in image recognition. In a convolutional layer, each neuron is connected only to neurons located within a small rectangle (or receptive field) in the previous layer (Figure 1). A convolutional layer is composed of several feature maps, and within each feature map, all the neurons share the same weight vector and bias. Each feature map applies the same convolution kernel (or filter) represented by the weight vector the size of the receptive field to all input connections of each of its neurons. During training, a CNN finds

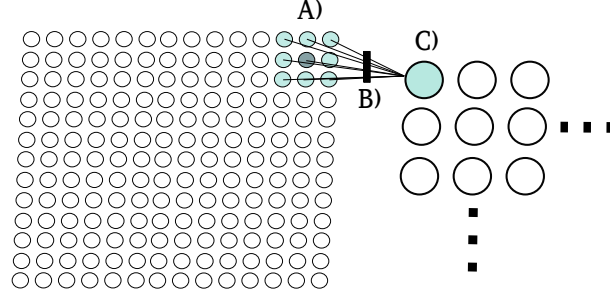


Fig. 1: Example convolution operation. A  $3 \times 3$  convolution kernel (A) is applied on the input layer, i.e. it is applied repeatedly over its receptive field (left). Each convolution kernel consists of a set of trainable weights optimized during backpropagation. The result of applying the kernel (B) is a single real number (C) in a convolutional layer that is commonly input to a pooling layer (not shown).

the most useful convolution kernels for its task and learns to combine them into more complex patterns.

Upon applying a convolution kernel, the convolutional layer's outputs are transformed by an activation function and then they are optionally merged by a pooling layer. The purpose of a pooling layer, which has no connection weights, is to down-sample the output of the previous convolutional layer. It aggregates its inputs using an aggregation function such as the max or avg, resulting in *max pooling layer* or *average pooling layer*. In a *max pooling layer*, only the maximum input value from each convolution kernel is transferred to the next layer, while all the other inputs are dropped. In an *average pooling layer*, the average of input values from all convolution kernels is transferred to the next layer. Thus, applying pooling layers allows us to reduce the input dimensionality and hence the memory and computing resources required by a neural network.

We use the following notation to describe the sequence of layers and operations that can be regarded as a single composite layer:

$$o_l = Pool(a(Conv(r, o_{l-1}, f)), s)$$

where a convolutional layer *Conv* is applied to the output  $o_{l-1}$  of the previous layer, followed by an activation function *a*, and a pooling layer *Pool* that returns  $o_l$  — the output of the composite layer *l*; *r* is the size of the convolution kernel, *f* is the number of convolution kernels (filters) or, equivalently, the number of feature maps, and *s* is the size of the pooling layer.

Deep neural network learning is prone to overfitting, that is, the network weights adapt to the training data too well. Dropout layers [33], which randomly discard a certain percentage of neurons in each training iteration, can solve this problem and improve the generalization performance of a neural network.

### 2.3 Node Ranking Algorithms

Node ranking algorithms assess the relevance of a node in a network either globally, relative to the whole network, or locally, relative to a sub-network by assigning a *score* (or a *rank*) to each node in the network.

A well known global node ranking algorithm is PageRank [34], which has been used in the Google search engine. Others include Weighted PageRank [35], SimRank [36], diffusion kernels [37], hubs and authorities [38], and spreading activation [39]. More recent network node ranking algorithms are the PL-ranking [40] and NCDawareRank [41]. Network nodes can also be ranked using network centrality measures, such as Freeman's network centrality [42], betweenness centrality [43], closeness centrality [44], and Katz centrality [45].

We consider local node ranking algorithms that compute a local relevance score of a node relative to a given subset of other nodes. A representative of this class of node ranking algorithms is the personalized PageRank (P-PR) algorithm [34], sometimes referred to as random walk with restart [46]. Personalized PageRank uses the random walk approach to calculate the relevance of nodes in a network. It measures the stationary distribution of a random walk that starts at node  $u$ . The algorithm at each iteration follows a random edge of the current node with a predefined probability  $p$  (usually set to 0.85), and with probability  $1 - p$  jumps back to the starting node. The P-PRS-based approaches were used successfully to study cellular networks, social phenomena [47], and many other real-world networks [48]. Efficient implementation of P-PRS algorithms remains an active research field. Recently, a bidirectional variation of the P-PRS was introduced, which significantly speeds up the node ranking process [49, 50].

The obtained stationary distribution of a random walk can be used directly for network learning tasks, as demonstrated in the recently introduced HINMINE methodology [51]. Our Deep Node Ranking algorithm uses both fast personalized node rank computations, and the semantic representation learning power of deep neural networks.

### 2.4 The Rationale Behind the Proposed Approach

As discussed in the previous sections, many of the current state-of-the-art network embedding algorithms based on deep learning suffer from high computational complexity due to exhaustive search of the hyperparameter space. The properties of multi-layered neural network architectures are not well understood and are commonly evaluated using grid search over various layer sizes and other hyperparameters, which is computationally inefficient.

The proposed DNR algorithm addresses these issues by exploiting the classification potential of the fast Personalized PageRank algorithm with shrinking, integrated with a neural network architecture. Compared to node2vec and similar methods, which build on simulated second order random walks, the proposed approach achieves similar predictive performance by using only the first order Markov dynamics, that is, random walkers with no memory. Further, the proposed algorithm enables for direct node classification, where node classes are obtained without the intermediary network embedding step characteristic of other

approaches. Development of algorithms which are linear in space with respect to the network size is a challenging task. The proposed algorithm is implemented using efficient sparse matrix manipulations, its space complexity is  $\mathcal{O}(|E| + |V|)$ , where  $|E|$  is the number of network edges and  $|V|$  is the number of vertices.

### 3 Deep Node Ranking Algorithm

We describe the novel Deep Node Ranking (DNR) algorithm for (semi-) supervised machine learning of complex networks (Figure 2).

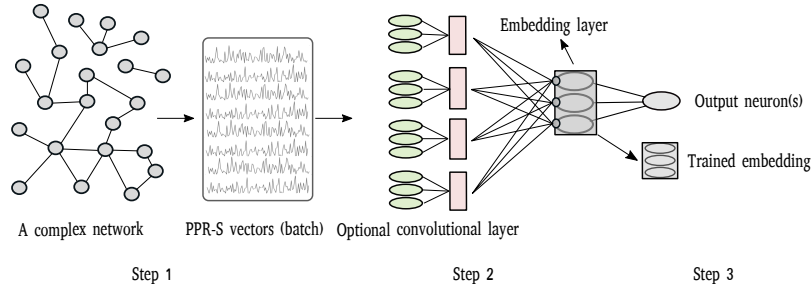


Fig. 2: Deep Node Ranking algorithm workflow. In the first step, personalized node ranks are computed for each network node resulting in the Personalized PageRank with Shrinking (P-PRS) vectors. Shrinking corresponds to efficient exploration phase during computation of PageRank vectors, and is in detail explained further in this work. In the second step, the P-PRS vectors enter a deep neural network consisting of one convolutional layer, and a dense embedding-producing layer, whose size equals to the predefined embedding dimension. The sizes of intermediary layer(s) are determined based on the sparseness of the input network and the dimension of the P-PRS vectors. The third, output step, consists either of an output layer with the number of its neurons equal to the number of target classes (top) enabling direct classification of nodes, or the embeddings (bottom), which correspond to the embedding layer from step 2. The embeddings can be used for downstream machine learning tasks, such as classification, network visualization and comparison.

An outline of the three steps of the proposed DNR algorithm is as follows.

1. Input Preparation. Learning node representations using the Personalized PageRank with Shrinking (P-PRS) algorithm, shown in Step 1 of Figure 2 and described in Section 3.1.
2. Neural Network Computation. A neural network architecture processes the prepared personalized page rank vectors, shown in Step 2 of Figure 2 and is described in Sections 3.2 and 3.3.



3. Different Outputs. The output of the network can be either a low-dimensional embedding of the network (Figure 2; Step 3, bottom), or node classification, that is, direct learning of node labels (Figure 2; Step 3, top).

In the next subsections, we provide the details of the steps outlined above.

### 3.1 Personalized PageRank with Shrinking Algorithm

The aim of the Personalized PageRank with shrinking (P-PRS) [52, 51] algorithm (Algorithm 1) is to obtain node representations (or P-PRS vectors) by simulating random walks for each node of the input network. Compared to the network adjacency matrix, these P-PRS vectors, one for each node, contain higher levels of network topology, and are more suitable for learning than the adjacency matrix.

The algorithm consists of two parts. In the first part (Shrinking; lines 9-24), the PageRank spreads from the nodes with non-zero PageRank values to their neighbors, in each iteration.

We take into account the following facts:

1. If no path exists between nodes  $u$  (the starting node) and  $i$ , the P-PRS value assigned to node  $i$  will be zero.
2. The P-PRS values for nodes reachable from  $u$  will be equal to the P-PRS values calculated for a reduced network  $G_u$ , obtained from the original network by only accounting for the subset of nodes reachable from  $u$  and connections between them (lines 27 to 36 in Algorithm 1).

If the network is strongly connected,  $G_u$  will be equal to the original network, yielding no change in performance to the original P-PR algorithm. However, if the resulting network  $G_u$  is smaller, the calculation of the P-PRS values will be faster as they are calculated on  $G_u$  instead of on the whole network. In our implementation, we first estimate if the network  $G_u$  contains less than 50% of the nodes of the whole network (lines 9-17 in Algorithm 1). This is achieved by expanding all possible paths from node  $i$  and checking the number of visited nodes in each step. If the number of visited nodes stops increasing after a maximum of 15 steps, we know we have found the network  $G_u$  and we count its nodes. If the number of nodes is still increasing, we abort the calculation of  $G_u$ . We limit the maximum number of steps because each step of computing  $G_u$  is computationally comparable to one step of the power iteration used in the PageRank algorithm [53] which converges in about 50 steps. Therefore we can considerably reduce the computational load if we limit the number of steps in the search for  $G_u$ .

In the second part of the algorithm (lines 25-42), node ranks are computed using the power iteration (Eq. 2), whose output consists of P-PRS vectors. For each node  $u \in V$ , a feature vector is computed by calculating the stationary distribution of a random walk, starting at node  $u$ . The stationary distribution

---

**Algorithm 1:** Personalized PageRank algorithm with shrinking [52].

---

```

1 Algorithm computeRankVectors: pseudocode of Personal PageRank
  algorithm with shrinking
  Data: A complex network's stochastic adjacency matrix  $A$ , its set of nodes  $V$ ,
    damping factor  $\delta$ , starting nodes  $n$ , number of all nodes  $|V|$ , spread step
     $\mathfrak{s}$  (default value 15), spread percent  $\mathfrak{p}$  (default value 50%)
  Result: transition probability vector  $\kappa$  for each node in  $n$  to all other nodes
2  $core\_vector := [0, \dots, 0](|V| - times)$ ; ▷ Initialization
3  $core\_vector[n] := 1$ ;
4  $core\_rank := \frac{core\_vector}{|n|}$ ;
5  $rank\_vector := \frac{core\_vector}{|n|}$ ;
6  $v := \frac{core\_vector}{|n|}$ ; ▷ Normalization.
7  $steps := 0$ ;
8  $nz := |n|$ ; ▷ Shrinking part.
9 while  $nz < |V| * \mathfrak{p} \wedge steps < \mathfrak{s}$  do
10    $steps := steps + 1$ ;
11    $v = v + A \cdot v$ ; ▷ Update transition vector.
12    $nzn := nonZero(v)$ ; ▷ Identify non-zero values.
13   if  $nzn = nz$  then
14      $shrink := True$ ;
15   end
16    $nz := nzn$ ;
17 end
18  $rr := [0, 1, \dots, |n|]$ ;
19  $toReduce := \mathbb{I}_{x>0}v$ ; ▷ Keep non-zero entries.
20 if  $shrink$  then
21    $core\_rank := core\_rank[toReduce]$ ;
22    $rank\_vector := rank\_vector[toReduce]$ ;
23    $A := A[:, toReduce][toReduce, :]$ ; ▷ Shrink a sparse adjacency array.
24 end
25  $diff := \infty$ ;
26  $steps := 0$ ; ▷ Node ranking - standard PageRank iteration
27 while  $diff > \epsilon \wedge steps < max\_steps$  do
28    $steps := steps + 1$ ;
29    $new\_rank := A \cdot rank\_vector$ ;
30    $rank\_sum := \sum_i rank\_vector_i$ ;
31   if  $rank\_sum < 1$  then
32      $new\_rank := new\_rank + start\_rank * (1 - rank\_sum)$ ;
33   end
34    $new\_rank := \delta * new\_rank + (1 - \delta) * start\_rank$ ;
35    $diff := ||rank\_vec - new\_rank||$ ; ▷ Norm computation.
36    $rank\_vec := new\_rank$ ;
37 end
38 if  $shrink$  then
39    $ret := [0, \dots, 0](n - times)$ ;
40    $ret[toReduce] := rank\_vec$ ;
41    $\kappa := (ret[n] := 0)$ ;
42 else
43    $\kappa := (ret[n] := 0)$ ;
44 return  $\kappa$ ;

```

---

is approximated by using power iteration, where the  $i$ -th component of the approximation in the  $k$ -th iteration is computed as

$$\gamma_u(i)^{(k+1)} = \alpha \cdot \sum_{j \rightarrow i} \frac{\gamma_u(j)^{(k)}}{d_j^{out}} + (1 - \alpha) \cdot v_u(i); k = 1, 2, \dots \quad (2)$$

The number of iterations  $k$  is increased until the stationary distribution converges to the stationary distribution vector (P-PRS value for node  $i$ ). In the above equation,  $\alpha$  is the damping factor that corresponds to the probability that a random walk follows a randomly chosen outgoing edge from the current node rather than restarting its walk. The summation index  $j$  runs over all nodes of the network that have an outgoing connection toward  $i$ , (denoted as  $j \rightarrow i$  in the sum), and  $d_j^{out}$  is the out degree of node  $d_j$ . The term  $v_u(i)$  is the restart distribution that corresponds to a vector of probabilities for a walker's return to the starting node  $u$ , i.e.  $v_u(u) = 1$  and  $v_u(i) = 0$  for  $i \neq u$ . This vector guarantees that the walker will jump back to the starting node  $u$  in case of restart<sup>6</sup>.

In a single iteration ( $k \rightarrow k + 1$ ), all the stationary distribution vector components  $\gamma_u(i)$  with  $i \in |V|$  are updated which result in the P-PRS vector  $\gamma_u^{(k+1)}$ . Increasing  $k$  thus leads to the  $\gamma_u^{(k)}$  eventually converging to the PageRank  $\gamma_u$  of a random walk starting from the node  $u$  (see Algorithm 1). The Eq. 2 is optimized using power iteration, which is especially suitable for large sparse matrices, since it does not rely on spatially expensive matrix factorization in order to obtain the eigenvalue estimates<sup>7</sup>.

The P-PRS algorithm simulates a first-order random walk in which no historical information is incorporated in the final stationary distribution. The time complexity of the described P-PRS algorithm with shrinking for  $k$  iterations is  $\mathcal{O}(|V|(|E| + |V|) \cdot k)$  for the whole network, and  $\mathcal{O}((|E| + |V|) \cdot k)$  for a single node (for proof see Appendix A). In terms of spatial complexity the P-PRS algorithm is linear with respect to the number of edges ( $\mathcal{O}(|E|)$ ) if the input is a sparse matrix.

The advantage of the deep neural network architecture, discussed in the following section is that it can learn incrementally, from small batches of the calculated P-PRS vectors. In contrast, the previously developed HINMINE approach [51] requires that all the P-PRS vectors for the entire network are calculated prior to learning, which is due to HINMINE using the  $k$ -nearest neighbors and the support vector machines classifiers. This incurs substantial space requirements as the P-PRS vectors for the entire network require  $\mathcal{O}(|V|^2)$  of computer memory. The DNR algorithm presented here uses deep neural network instead, which can take as input small batches of P-PRS vectors. Therefore, only a small percentage of the vectors needs to be computed before the second step of the

<sup>6</sup> If the binary vector was composed exclusively of ones, the iteration would compute the global PageRank vector, and Eq. 2 would reduce to the standard PageRank iteration.

<sup>7</sup> The power iteration (Equation 2) converges exponentially, that is, the error is proportional to  $\alpha^k$ , where  $\alpha$  is the damping factor and  $k$  is the iteration number.

algorithm, learning the neural network, can begin. This offers significant improvement in both spatial and temporal complexity of the learning process. The time complexity is improved, since the learning part, which is performed on a GPU, can proceed simultaneously with the P-PRS computation, which is done on a CPU.

### 3.2 Optimization of the Deep Neural Network Architecture

In this section, we systematically evaluate different neural network architectures to arrive at the optimized architecture topology used in the final DNR algorithm. The rest of this section is structured as follows. First, we discuss the validation scheme used to optimize the architecture topology. Next, we investigate how different activation functions impact the selected architecture’s performance. We additionally explore the possibility of using convolutions over P-PRS vectors directly, and conclude with a general formulation of the architecture that we finally test on unseen networks.

**Hyperparameters Optimization.** We optimized the following hyperparameters of the neural network architecture for the task of node classification: the number of training epochs and the activation functions. Here, node can be labeled with one or more labels, and the neural network is trained to predict the labels as correctly as possible. Hyperparameter optimization was performed on the *Homo sapiens* protein interaction network, whereas subsequent parameter tuning concerning weight matrices and bias vectors was performed for each new network separately. The *Homo sapiens* protein interaction network (see Section 4) was split into a training set (10% of nodes) and a validation set (90% of nodes) as done in [7, 54] and later in [4] — the classification performance was evaluated by training a logistic regression classifier on the obtained embedding, so that from 10% up to 90% of embedded nodes were used for training.

In Ref. [7] it is not specified how the nodes used for embedding construction are dealt with in the validation phase. We believe that the nodes used for training the architecture should all be excluded from the validation phase. Therefore, the 10% of nodes that were used for hyperparameter tuning were always removed in the validation phase, in which the obtained embedding was used for node classification. This allowed us to avoid over fitting and assured fair comparisons.

The purpose of hyperparameter optimization was to make the performance of the evaluated intermediary architectures comparable to the current state-of-the-art [4, 7]. The hyperparameters defining the neural network architecture were optimized on a single validation data set, the *Homo sapiens* network. The performance of the hyperparameters optimized on the *Homo sapiens* network were then tested on new networks from different domains that were previously not seen by the neural network. In tests, the hyperparameters were *transferred* to the new networks, but parameters (weight matrices and bias vectors) were re-trained for each new network separately.

**Deep Neural Network Architecture.** In this section we demonstrate how a single hidden layer neural network was optimized to learn from P-PRS vectors. We chose a single-hidden layered network architecture based on the recent findings on deeper architectures ([11]) showing that shallow architectures are well suited for graph learning tasks. This general architecture, in this work termed DNR, is formulated as:

$$l_2 = \sigma(w_2(a(w_{\text{dim}}X + b_{l_1})) + b_{l_2});$$

where  $X$  corresponds to the input of the neural network, which are the P-PRS vectors generated in the input preparation phase,  $l_1$  is the first and only hidden layer (the embedding layer),  $l_2$  is the output layer whose number of neurons is equal to the number of target classes, and  $a$  is one of the standard activation functions (discussed later; see Table 1). The hidden layer size  $\text{dim}$  is the dimension of the embedding, which is set to the value of 128 in this work as was also done in [5, 4, 54]. The deep neural network evaluated was trained using the Adam optimizer [32], a version of stochastic gradient descent using the binary cross-entropy loss function [8]. For the following experiments, we varied the amount of the nodes used for training the architecture from 10% to 90% using 10% steps. The performance curves show the average performance with respect to the percent of nodes used for training, as well as the variability of different architectures tested (see Figure 3).

**Activation Function Selection.** We tested several different activation functions listed in Table 1.

Table 1: Activation functions considered in the first hidden layer.

Activation function	Definition
Elu	$Elu(x) = \begin{cases} x, & \text{for } x \geq 0 \\ c(e^x - 1) & \text{for } x < 0 \end{cases}$
ReLU	$ReLU(x) = \begin{cases} 0, & \text{for } x < 0 \\ x & \text{for } x \geq 0 \end{cases}$
Leaky ReLU	$LReLU(x) = \begin{cases} 0.01x, & \text{for } x < 0 \\ x & \text{for } x \geq 0 \end{cases}$
Logistic ( $\sigma$ )	$\sigma(x) = \frac{1}{1+e^{-x}}$

The functions listed in the table are applied to every component of the input vector. The results in Figure 3 and Table 2 show the performance of a single-hidden layered neural network architecture with respect to different activation functions used.

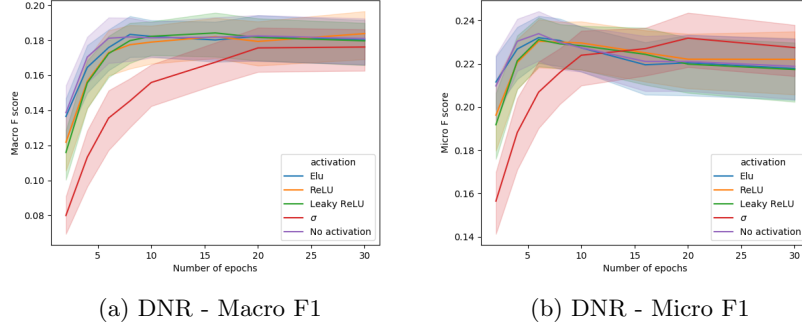


Fig. 3: Dependence of the architecture’s performance with respect to the number of training epochs. The confidence intervals are plotted based on 10 repetitions of the learning.

Having fixed the  $c$  parameter of Elu to 0.01, we observed that Leaky ReLU, ReLU, as well as Elu functions performed better compared to the  $\sigma$  activation function in the first  $\approx 20$  epochs. This indicates the convergence rate of the sigmoid activation is slower. For the further experiments, we selected the ReLU activation function, due to its fast and robust convergence (see Figure 3). We next investigated how the dimensionality of the input P-PRS vectors could be reduced prior to expensive training of the dense layers.

Table 2: Macro and Micro F1 averaged performance with respect to number of training epochs for the DNR architecture.

Epochs	Macro F1					Micro F1				
	$\sigma$	Elu	LReLU	None	ReLU	$\sigma$	Elu	LReLU	None	ReLU
2	0.080	0.136	0.116	<b>0.139</b>	0.122	0.157	<b>0.212</b>	0.192	0.210	0.196
4	0.113	0.164	0.156	<b>0.170</b>	0.157	0.188	0.227	0.221	<b>0.230</b>	0.221
6	0.136	0.176	0.172	<b>0.181</b>	0.173	0.207	0.232	0.231	<b>0.234</b>	0.230
8	0.145	<b>0.183</b>	0.180	0.182	0.177	0.216	<b>0.231</b>	0.229	0.230	0.230
10	0.156	<b>0.182</b>	<b>0.182</b>	0.181	0.179	0.224	0.227	0.228	0.227	<b>0.230</b>
16	0.167	0.180	<b>0.184</b>	0.182	0.182	<b>0.227</b>	0.220	0.224	0.221	0.225
20	0.176	<b>0.182</b>	<b>0.182</b>	<b>0.182</b>	0.179	<b>0.232</b>	0.220	0.220	0.221	0.222
30	0.176	0.180	0.180	0.181	<b>0.184</b>	<b>0.227</b>	0.218	0.217	0.219	0.222

These initial experiments demonstrate that the DNR architecture becomes saturated at  $\approx 15$  epochs. In the following experiments, we consider 15 epochs as the standard training time. After initial boost in performance, the network appears to over fit, as its performance gradually decreases (Fig. 3).

**Convolutions Over Stationary Distributions.** The input P-PRS input vectors can be high dimensional leading to a large spatial complexity of the current approach. To improve the performance, we introduced an additional convolutional layer using 1D convolution over the P-PRS input vectors, that is, the *1D average pooling* function, to reduce their dimensionality. The experiments were performed using the best-performing architecture (see previous subsections) consisting of a single hidden layer ( $\text{dim} = 128$ ) and the *ReLU* activation function. We tested the effect of the convolutional layer as follows.

We explored how different parametrizations of the convolution and pooling influence the performance of the architecture by varying the three parameters determining the convolutional layer, which are, the number of filters, the kernel size, and the pooling region size. As the features of the P-PRS input vectors are inherently unordered, each convolution parametrization was subject to perturbation testing. For each parametrization, we generated 20 different feature orderings and averaged the Macro and Micro F1 scores obtained using 50% of vectors for training the logistic regression classifier (see Section 3.2). Each parametrization was trained for 15 epochs, as we observed the saturation point for this architecture closely follows the one without convolutions (Fig.3). For this experiment, we varied the kernel size, the number of filters and the size of the pooling region over the following interval:  $[2, 8, 16, 64, 128, 512]$ . In total, we tested 1,944 configurations. The summarized results of this experiment are given in Table 3.

Table 3: Performance of different convolution layer parametrizations. For readability, each parameterization consists of a triplet  $(f, k, p)$ , where  $f$  denotes the number of filters,  $k$  the kernel size and  $p$  the pooling size. We list triplets sorted by both micro, as well as macro F1 performance.

Convolution parameterization	Macro F1	Micro F1
No convolution	0.183	<b>0.238</b>
(2,8,2)	<b>0.184</b>	0.223
(2,2,2)	0.175	0.227
(2,8,2)	0.179	0.217
(8,2,2)	0.182	0.216
...		
(2,64,128)	0.061	0.167
(2,2,512)	0.060	0.166

These experiments showed that large kernel sizes, as well as pooling regions decrease the performance. However, small convolution windows (e.g., (2,8,2)) could be used to reduce the parameter space and hence speed up the training, and foremost to reduce the space requirements of the neural network.

The (2, 8, 2) architecture was next assessed for the effect of different activation functions (Table 4 and Figure 4). Here, similarly to the non-convolutional

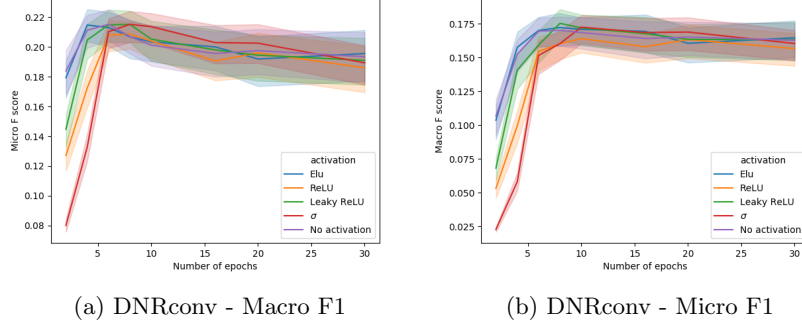


Fig. 4: Dependence of the (2,8,2) architecture performance with respect to the number of training epochs. The learning pattern is similar to the one observed in Fig. 3

architecture in the previous section, we varied the number of epochs and different activation functions. Note that the table shows only the selected epoch numbers for readability purposes, whereas Fig. 4 shows results of exhaustive search with the increment of two epochs.

Table 4: Micro and Macro F1 averaged performance with respect to number of training epochs for the DNRconv architecture.

Epochs	Macro F1					Micro F1				
	$\sigma$	Elu	LReLU	None	ReLU	$\sigma$	Elu	LReLU	None	ReLU
2	0.023	0.104	0.068	<b>0.107</b>	0.053	0.080	0.179	0.145	<b>0.184</b>	0.127
4	0.058	<b>0.158</b>	0.141	0.153	0.100	0.133	<b>0.215</b>	0.205	0.211	0.173
6	0.152	<b>0.170</b>	0.159	<b>0.170</b>	0.155	0.210	0.213	<b>0.215</b>	<b>0.215</b>	0.208
8	0.160	0.172	<b>0.175</b>	0.170	0.160	<b>0.215</b>	0.207	<b>0.215</b>	0.207	0.209
10	<b>0.173</b>	0.171	0.172	0.169	0.164	<b>0.214</b>	0.203	0.205	0.201	0.204
16	<b>0.169</b>	<b>0.169</b>	0.168	0.164	0.158	<b>0.203</b>	0.200	0.198	0.196	0.191
20	<b>0.169</b>	0.161	0.164	0.165	0.163	<b>0.203</b>	0.192	0.195	0.198	0.196
30	0.161	<b>0.165</b>	0.163	0.163	0.157	0.189	<b>0.196</b>	0.191	0.193	0.186

The experiments with DNRconv architecture indicate, use of convolutions diminishes the (Macro F1) performance, yet remains a viable alternative for reduction of spatial complexity. Note that the version of DNR with convolutions can be stated as:

$$l_2 = \sigma(w_2(a(w_{\text{dim}} \text{Conv1D}(X, f, k, p) + b_{l_1})) + b_{l_2});$$



where  $\text{Conv1D}(X, f, k, p)$  corresponds to one dimensional convolution, parameterized with the number of filters ( $f$ ), kernel ( $k$ ) and pooling ( $p$ ) size, over the P-PRS vector(s)  $X$ . In the remainder of this work we report experiments using non-convolutional DNR architecture as well as using the  $(2, 8, 2)$  convolutional architecture. The resulting neural networks are trained in mini batches, consisting of P-PRS node rank vectors. The weights of the DNR architecture are thus *shared* between *all* nodes.

### 3.3 Three types of learning supported by DNR

Having described the neural network architecture, trained on the P-PRS vectors, we further discuss how the architecture can be used for different network learning tasks.

**Supervised construction of a network embedding** Having defined the general neural network architecture, we present the details of its implementation using stochastic mini-batch approach. Hence the final result of the procedure explained in this section are node embeddings which include *partial information* on node labels, obtained via the proposed architecture. As the training of deep neural networks proceeds in batches, and we do not need to provide the whole data set as the input at the same time—we propose a minibatch implementation from node rank vector construction step onwards. Using smaller batches of P-PRS vectors as inputs, the spatial requirements of the DNR are in the order of  $\mathcal{O}(|V| + |E|)$ . All steps of the proposed implementation can run in parallel, partially on CPUs and partially the GPU(s). The pseudocode is presented in Algorithm 2.

The proposed algorithm iterates through two main steps. First, personalized node ranks (as computed with Algorithm 1) are computed for a subset (batch) of nodes. The obtained  $|N| \cdot \beta$  matrix ( $\beta$  represents the batch size) is used as input to the proposed neural network architecture. Due to the fact that learning is carried out only on a subset of nodes, weights of the deep architecture are updated only for nodes, considered in the training phase (e.g., 10 % of all nodes). When all such nodes are used, the obtained architecture is used to map P-PRS node representations (of size  $|N|$ ) into a node embedding of size  $\text{dim}$ . Once encoded, the obtained embedding ( $\psi$ ) is returned as the output.

To make the pseudocode better comprehensible, we omitted the following details related to parallel processing of the node stream. First, after the deep architecture is trained, not all nodes in the final batch are necessarily used for training ( $|train| < \text{trainSamples}$ ). The remainder of the nodes is thus embedded using the trained encoder architecture. Note that the number of such P-PRS vectors is at most the size of a single batch. Further, as the embedding construction is based on a small percentage of all nodes (e.g., 10%), the P-PRS vectors representing these nodes are during training of the neural network stored in a Hadoop sparse matrix [55], and as such do not represent a spatial drawback.

---

**Algorithm 2:** Deep Node Ranking pseudocode. First, rank vectors are computed for individual batches. A low percentage of the vectors is used to train the model. Once trained, the model is used to construct embeddings of the network's nodes.

---

```

1 Algorithm DNR: pseudocode of Deep Node Ranking
   Data: A complex network  $Q$ , its set of nodes  $N$ , set of labels  $L$ , parallel batch
           size  $\lambda$ , train percent  $\Phi$ 
   Result: low-dimensional network node embedding  $\psi$ 
2  $train := \emptyset$ ;
3  $trainSamples := \lceil \Phi |N| \rceil$ ;
4  $batches := \{\{N_{i, \dots, i+\lambda}\} | i \in [0, |N|, \lambda]\}$ ;
5 foreach  $batch \in batches$  do
6   do parallel  $q \in batch$ 
7      $q_{rank} := computeRankVectors(q)$ ; ▷ P-PRS iteration.
8   end
9   foreach  $q \in batch$  do
10    if  $|train| < trainSamples$  then
11       $train := train \cup \{q_{rank} | q \in batch\}$ ; ▷ Build training set.
12    else
13      if not yet trained then
14        do
15           $trainDeepArchitecture(train)$ ; ▷ Compute embedding.
16        while  $epochs$ ;
17      if batch not embedded then
18        foreach  $q \in batch$  do
19           $lowDimensionalVector :=$ 
20             $predictWithDeepArchitecture(q_{rank})$ ;
21           $\psi := \psi \cup lowDimensionalVector$ ; ▷ Main result (1).
22        end
23      else
24         $lowDimensionalVector :=$ 
25           $predictWithDeepArchitecture(q_{rank})$ ;
26         $\psi := \psi \cup lowDimensionalVector$ ; ▷ Main result (2).
27      end
28    end
29  end
30 end
31 return  $\psi$ ;

```

---

The proposed architecture is an improvement over a naïve approach, where all node ranks are first computed, and only then fed into the deep architecture ( $\mathcal{O}(|V|^2)$ ) memory.

**End-to-end learning of node labels** In the previous subsection, we discussed how the Deep Node Ranking approach can be used to obtain a node embedding

using a small subset of labeled nodes. In this section we continue with *end-to-end* learning of node labels.

Formally, the constructed classification model approximates the mapping  $\tau : N \rightarrow c \in [0, 1]^{|V| \times |C|}$ , where  $N$  represents a network's set of nodes,  $C$  a set of class values and  $c$  a single vector of node classes. Note that the class matrix  $[0, 1]^{|V| \times |C|}$  here corresponds to the probabilities of classes for each node. In this case, the neural network is trained as any standard machine learning algorithm in a semi-supervised setting, where the node ranks are initially computed. The architecture formulation and other parameters remain the same as described in Section 3.2.

**Unsupervised learning** So far Deep Node Ranking was used in supervised setting for learning node labels. DNR can also be useful for unsupervised representation learning, useful when visualizing and comparing complex networks. We can achieve this by using the architecture discussed in Section 3.2. The only difference we introduce is that we replace the target classes with the input, i.e. the vectorized network itself. Note that the obtained auto encoder architecture is formally undercomplete [8], as  $\dim < |V|$ , i.e., the embedding dimension is of lower dimensionality than the input vectors. The proposed unsupervised setting is explored as part of the qualitative, as well as quantitative evaluation, where obtained representations are used for network visualization and node classification.

**Number of parameters** A relevant aspect in studying neural network performance is the total number of trainable parameters. In this section we prove that the number of parameters scales linearly with the number of a network's nodes, should all nodes be taken into account during P-PRS construction.

**Proposition 1.** *The total number of parameters is linear with respect to the number of nodes, used for P-PRS construction, i.e.  $p = \mathcal{O}(|V|)$ , where  $p$  corresponds to the number of parameters.*

The P-PRS vectors obtained prior to architecture training are in this work of dimensionality  $|V|$ . Consider an architecture with a single hidden layer consisting of  $\dim$  neurons (size of the embedding dimension), and  $C$  target classes. The total number of parameters  $p$  for such architecture is

$$p = |V| \cdot \dim + C \cdot \dim = \mathcal{O}(|V|).$$

The total number of trainable parameters is sub-linear with respect to the number of nodes, if the P-PRS vectors' sizes *are reduced* prior to being used as input to the dense (embedding) layer. In this work, we propose the use of convolution operator for such cases, however, Some form of e.g., streaming PCA could also be used for this purpose.

## 4 Data sets and experimental setting

In this section we first describe the data sets used, followed by the experimental settings and a short description of compared approaches.

### 4.1 Data sets

We evaluate the proposed approach on nine real-world complex networks which is one of the largest collections of complex networks formulated as multi-label classification task. The *Homo Sapiens* (proteome) [56], POS tags [57] and Blogspot data sets [58] are used in the same form as in [4]. The existing data sets we use are:

- The *Homo sapiens* data set represents a subset of the human proteome, i.e., a set of proteins which interact with each other. The sub-network consists of all proteins, for which biological states are known [59]. The goal is to predict protein function annotations. This data set was used as validation data set, hence its results are not included in the testing phase, yet are visualized along other micro and macro F1 curves for comparison.
- The POS data set represents part-of-speech tags obtained from Wikipedia—a co-occurrence network of words appearing in the first million bytes of the Wikipedia dump [57]. Different POS tags are predicted.
- The Blogspot data set represents a social network of bloggers (Blogspot website) [58]. The labels represent blogger interests inferred through the metadata provided by the bloggers.
- The CiteSeer citation network consists of scientific publications classified into one of six classes (categories). [60].
- The Cora citation network consists of scientific publications classified into one of seven classes (categories). [60].
- The E-commerce network is a heterogeneous network connecting buyers with different products. As the DNR methodology proposed in this work operates on homogeneous networks only, this network was prior to learning transformed using term frequency weighting scheme. The paths used for obtaining a homogeneous network all consisted of

$$Person \xrightarrow{purchased} \{A,B,C\}\text{-level item} \xrightarrow{purchasedBy} Person$$

triplets.

We refer the interested reader to [51] for detailed description of the data set and its transformation to a homogeneous network. The two classes being predicted correspond to genders of buyers.

One of the main contributions of this work are also three novel node classification data sets, we obtained as follows.

- Two data sets related to Bitcoin trades [61] are used. The two networks correspond to transactions within two different platforms, namely Bitcoin OTC and Bitcoin Alpha. Each edge in these network represents a transaction, along with an integer score in range  $[-10, 10]$ , (zero-valued entries are not possible). We reformulate this as a classification problem by collecting the trust values associated with individual nodes and considering them as target classes. The resulting integer values can thus belong to one of the 20 possible classes. Note that more than a single class is possible for individual node, as we did not attempt to aggregate trust scores for individual nodes.
- The Ions data set is based on the recently introduced protein-ion binding site similarity network [62]. The network was constructed by structural alignment using ProBiS family of algorithms [63, 64, 65] where all known protein-ion binding sites were considered. The obtained network was pruned for structural redundancy as described in [62]. Each node corresponds to one of 12 possible ions and each weighted connection corresponds to the ion binding site similarity between the two considered networks.

The data sets are summarized in Table 4.1. Apart from existing, well known benchmark data sets, we compiled three novel network classification data sets with distinct topological properties (two Bitcoin and the Ion network), which the community can use in further studies. Links to the data sets, along with other material presented in this paper is given in Section 6.

Table 5: Networks used in this study and their basic statistics. The CC denotes the number of connected components. The clustering coefficient measures how nodes in a graph tend to cluster together, and is computed as the ratio between the number of closed triplets and the number of all triplets. The network density is computed as the number of the actual connections, divided by all possible connections. The mean degree  $\overline{Deg}$  corresponds to the average number of connections of a node.

Name	Classes	Nodes	Edges	CC	Clustering	Density	$\overline{Deg}$
Citeseer	6	3,327	46,76	438	0.141471	0.000845	2.810941
Bitcoin Alpha	20	3,783	14,124	5	0.17662	0.001974	7.467090
Ions	12	1,969	16,092	326	0.528704	0.008306	16.345353
Homo Sapiens	50	3,890	38,739	35	0.146449	0.005121	19.917224
Cora	7	2,708	5,278	78	0.240673	0.001440	3.898080
Blogspot	39	10,312	333,983	1	0.463196	0.006282	64.775601
Bitcoin	20	5,881	21,492	4	0.177504	0.001243	7.308961
POS	40	4,777	92,517	1	0.538570	0.008110	38.734352
Ecommerce (tf)	2	29,999	178,608	8,304	0.484108	0.000397	11.907597

## 4.2 Experimental setting

In this section we describe the experimental setting, used to evaluate the proposed method against selected baselines. The parameterization of the DNRconv is as follows. For the *Elu* activation function we fixed the  $c$  parameter to 0.01. The number of training epochs was initially set to 20 for all data sets. For embedding-based methods, we consider 20% of the data set for supervised embedding construction. This part of the data set is later omitted from the testing phase. We shall also test if we would get better results if we used these 20% for learning directly (increasing the training data), without embedding phase (end-to-end learning).

Once we obtained the deep learning based network embeddings, the classification based on them used the L2-regularized logistic regression. Results for individual classes were merged by computing the micro and macro  $F_1$  scores. These two measures are used, as they have been used in the majority of other node classification studies [22, 4, 7, 54]. The  $F_1$  score of a class is defined as

$$F_1 = 2 \frac{\text{precision} * \text{recall}}{\text{precision} + \text{recall}}$$

Macro  $F_1$  score is defined as the average  $F_1$  score for all classes values  $\mathfrak{C}$ , i.e.

$$\text{macro}F_1 = \frac{\sum_{i \in \mathfrak{C}} F_{1_i}}{|\mathfrak{C}|};$$

whereas the micro  $F_1$  score is defined by counting global true positives (TP), false negatives (FN) and false positives (FP). The definition is then similar to ordinary  $F_1$  score, i.e.

$$\begin{aligned} \text{Micro}F_1 &= 2 \frac{\frac{\sum_{l \in \mathfrak{C}} TP(l)}{\sum_{l \in \mathfrak{C}} TP(l) + FP(l)} * \frac{\sum_{l \in \mathfrak{C}} TP(l)}{\sum_{l \in \mathfrak{C}} TP(l) + FN(l)}}{\frac{\sum_{l \in \mathfrak{C}} TP(l)}{\sum_{l \in \mathfrak{C}} TP(l) + FP(l)} + \frac{\sum_{l \in \mathfrak{C}} TP(l)}{\sum_{l \in \mathfrak{C}} TP(l) + FN(l)}} \\ &= 2 \frac{\text{precision}_{global} * \text{recall}_{global}}{\text{precision}_{global} + \text{recall}_{global}}. \end{aligned}$$

Due to many comparisons, we utilize the Friedman's test with Nemenyi post hoc correction to compute statistical significance of the differences. Results are visualized as critical distance diagrams, where ranks of individual algorithms according to scores across all data set splits are presented [66].

All experiments were conducted on a 64GB of RAM, 6 core Intel(R) Core(TM) i7-6800K CPU @ 3.40GH machine with a Nvidia 1080 GTX GPU. The HIN-MINE decomposition uses packages Networkx [67] and Numpy [68] for numerical and network-based tasks, respectively. Network statistics and visualization are implemented as part of the Py3plex library [69]. Node ranking is implemented using sparse matrices from the Scipy module [70] and TensorFlow library [26]. We leave re-implementation using recently introduced sparse tensor algebra on

GPUs for further work. The DNR architectures were trained with a stopping criterion of 5, i.e. if after three epochs performance remained the same, the training was terminated.

### 4.3 Free parameters of DNR

In this section, we discuss the parameters, which can be subject to problem-specific tuning. The parameters of the deep architecture, proposed in the last sections are:

- Number of epochs. The number of weight update cycles. For all experiments, this parameter was set to 20.
- Batch size. This parameter specifies how many P-PRS vectors are fed into the architecture simultaneously. The computation speed highly depends on this parameter, as batches are processed in parallel. For all experiments, this parameter was set to 10.
- P-PRS algorithm parameters:
  - $\epsilon$ . The error bound, which specifies the end of iteration. In this work set to  $10^{-6}$
  - Max steps. The number of maximum steps allowed during iteration. In this work set to 100,000
  - Damping factor. Probability, that the random walker continues at a given step. In this work set to 0.5
  - Spread step. Number of iteration steps allowed for the shrinking part. In this work set to 10.
  - Spread percent. Maximum percentage of the network to be explored during shrinking. In this work set to 0.3.

The DNR's parameters were hence set based entirely on the validation network (Homo Sapiens) , and are not optimized for each test network separately. As discussed, we intentionally do not perform hyperparameter tuning for each network, to showcase the general performance of the proposed algorithm.

### 4.4 The DNR implementations tested

We test the proposed approach against ten different baselines. We implement both variations of the proposed algorithm, i.e. the variant where the embedding is first constructed, and the variant, where the labels are learned directly. The DNR denotes the implementation, where embedding is first constructed, and then used for classification. The DNRconv denotes the DNR approach with added initial convolution layer, consisting of 2 filters, kernel size of 8 and average pooling region of 2. The DNR-e2e denotes end-to-end variants of the algorithm, where the train-test splits used by logistic regression classifier for learning from embeddings are used to learn from P-PRS vectors directly. Finally, both DNR as well as DNRconv were trained as autoencoders to test the effect of adding labels during training. The two architectures are termed autoDNRconv and autoDNR, respectively.

#### 4.5 The baseline approaches

HINMINE denotes the original HINMINE approach, where the resulting embedding is of dimension  $|N|^2$ . Additionally, using PCA we reduce this embedding to 128 dimensions—this variation is labeled HINMINE-PCA. Other baselines include the LINE algorithm—one of the first network embedding algorithms [22], Label Propagation (LP) [71, 51] and the *C++* version of the node2vec algorithm, compiled on the machine where benchmarks were evaluated. For node2vec, the same exhaustive search options were used as in the original paper [4]. Finally, we explore how P-PRS vectors can be compressed using non-negative matrix factorization (NNMF). For this task, we use of-the-shelf NNMF implementations, available as part of the Scikit-learn repository [72]. We use the following initializations. The NNMF (r) corresponds to random initialization, NNMF (svd) to standard Nonnegative Double Singular Value Decomposition, NNMF (svdar) for a variant, where zeros are replaced with small random numbers, otherwise the initialization is the same as NNMF (svd), and NNMF (svda) is a variant, where zeros are filled with the average of the input matrix. We introduce these additional experiments, so that PCA-based decomposition can be compared with computationally more demanding NNMF—to our knowledge we are the first to perform such experiments. The NNMF implementations are discussed in detail in [73].

#### 4.6 Other constraints

Note that the amount of RAM available for all approaches was 64GB. Should this amount be exceeded, the run is marked as unsuccessful. Further, we gave each algorithm at maximum five hours for learning. We selected these constraints, as the networks used are of medium size, and if a given method can not scale on these networks, it will not scale on larger e.g., social networks with millions of nodes and tens of millions, or even billions of edges.

### 5 Results and Discussion

In this section, we present the empirical results and discuss their qualitative as well as quantitative aspects. We first present results obtained for the node classification task, carried out on the data sets described in the previous section. Next, we qualitatively evaluate the proposed DNR algorithm for the task of node visualization.

#### 5.1 Classification Performance

In this section we first present the classification results in form of critical distance diagrams. Next, results are visualized over individual train percentages. Finally, Bayesian classifier comparison results are presented.

The best performing approach is DNR-e2e, a single hidden layer end-to-end Deep Node Ranking classifier. It outperforms existing state-of-the-art algorithms



by up to 8%. We present the performance of the algorithms in form of critical distance diagrams [66] (Figures 5 and 6) for readability purposes, full results in the tabular form are given in Appendix B. In these diagrams, algorithm's mean performance is displayed along a simple line with marked total ranks. If two algorithms perform (statistically) the same, they are connected with a bold line.

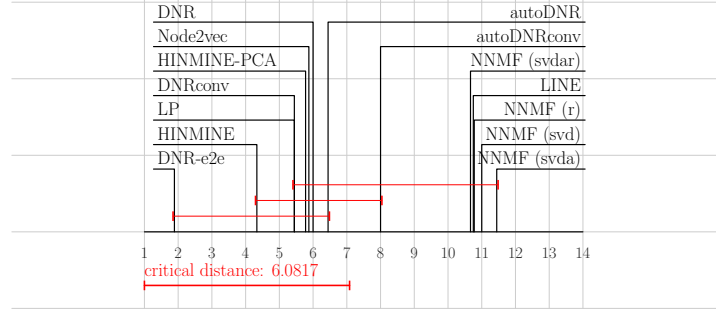


Fig. 5: Macro F1 CD diagram.

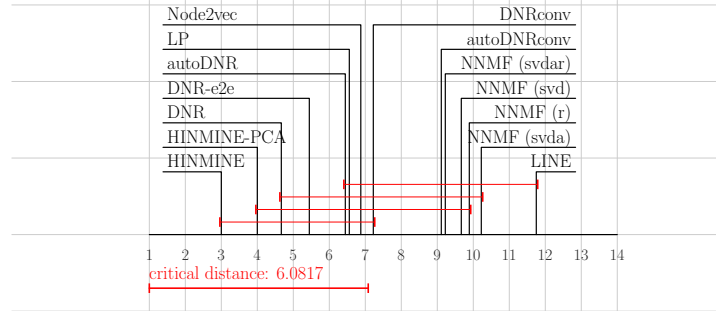


Fig. 6: Micro F1 CD diagram.

The DNR classifiers perform similarly to node2vec. The DNR approach, based on the Laplacian matrix performs worst for majority of the data sets. This indicates the merit of the initial phase of P-PRS node ranks. The HINMINE-based classification is one of the best-performing ones, indicating that the information from the whole network can offer similar results to simulated second order random walkers (node2vec). The results indicate, shallow deep architectures are well suited for learning from complex networks. A similar observation was made by [11], where shallow networks outperformed deeper ones. This might be the

result of locality of information in used graphs, i.e. no long paths are important for used classification task. We leave confirmation of this hypothesis for further work. Our results show that the DNR-based approaches are always present amongst top three classifiers. We observe there exists no significant difference between the DNR-based embeddings and Node2vec embeddings.

We continue the discussion by interpretation of results for all nine data sets (Figures 8 and 7). Note that the first data set (Homo sapiens) was used for validation, hence results obtained on this data set were not included in construction of CD diagrams. We observe that label propagation (LP) algorithm is strongly dependent on the network’s topology, as its performance is subject to high variability. This behavior is expected, as the LP algorithm works by moving through the network naïvely, meaning that its classifications can be biased to denser parts of networks. The DNR-based embedding approach performs similarly to the state-of-the-art node2vec algorithm. As stated previously, DNR-e2e, i.e. an architecture with a single hidden layer and end-to-end training outperforms other approaches. The HINMINE-PCA approach performs similarly to the original HINMINE methodology, indicating that raw node rank vectors can be reduced using fast PCA [74] projections. As there exist batch variants of PCA algorithms [75], the spatial complexity of the original HINMINE can also be reduced by using, similarly to the proposed DNR, minibatches of node rank vectors, we leave such experiments for further work. Experimental measurements indicate that the Cora data set is subject to the highest performance variability—the factorization-based approaches tend to be competitive with other approaches only when larger portions of the embedding are used for prediction.

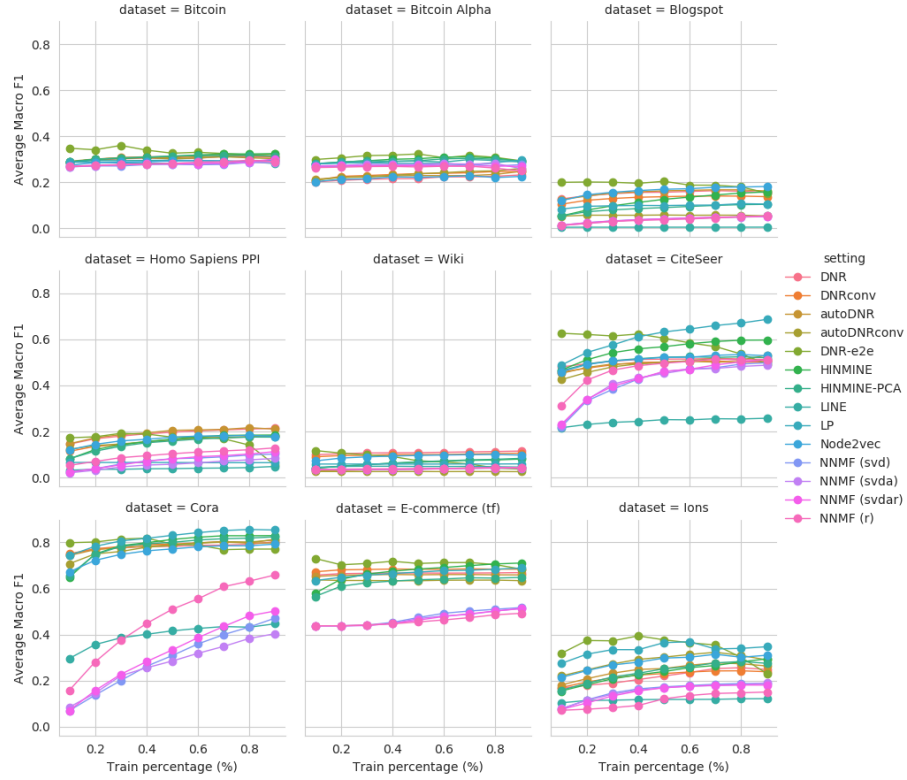


Fig. 7: Classifier performance (macro F1 scores).

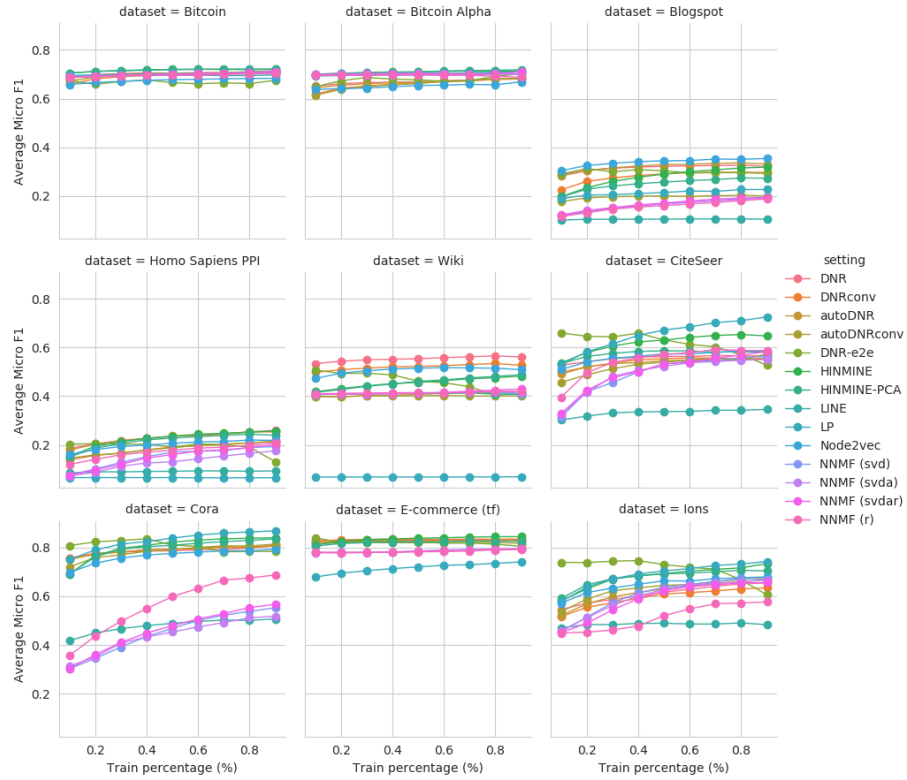


Fig. 8: Classifier performance (micro F1 scores).

The embedding-based approaches are more consistent—no large variation in classification performance is observed. We believe that this behavior is due to efficient sampling schemes used for embedding construction. Large deviations in performance mostly occur for Laplacian-matrix-based classifiers. This indicates that using only Laplacian matrix of a network is not sufficient input for (deep) learning part.

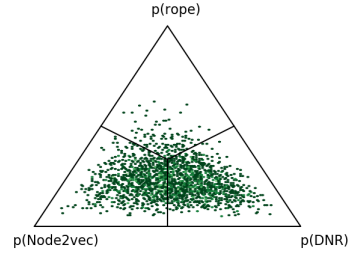
A more recent variant of the critical distance diagrams is that of Bayesian multiple classifier comparison [76]. Here, the Bayesian variant of the hierarchical t-test is used to determine differences in performance of given classifiers<sup>8</sup>. The idea of this test is, that it samples pairs of results, and is potentially more robust than classical CD diagrams. As Bayesian multiple classifier correction cannot be intuitively visualized for more than three classifiers, we focused on the two best-performing embedding approaches. We further compared performance of node2vec against the proposed DNR. We performed hierarchical t-test variant originally introduced by [76] (Figure 9).

The shown results were obtained as follows. Differences of classifiers' performances are given as input for each train percentage (10 repetitions). We subtract the performance of the second classifier from the one of the first. Hence, negative differences indicate superior performance of the left classifier and vice versa. The  $p(\text{rope})$  represents the equal success of the two classifiers. In the tests performed, we set the rope parameter to 0.01, meaning that the classifier's performance is considered the same, if it does not differ by more than 0.01. Note that default test settings were used for hierarchical sampling. The results can be interpreted as follows. Each green dot located within triangles represents a sample, obtained from the hierarchical model. As the sampling procedure is governed by the underlying data, green dots fall under one of the three categories; classifier one (dominates left), classifier two (dominates right), or none of the classifiers (dominates up). Upon model convergence, highest density of the green dots corresponds to higher probabilities of the observed classifier outperforming the alternative. As already observed using critical distance diagrams, embedding-based classifiers perform similarly—the green dots are approximately uniformly distributed between the left and the right parts of the triangle. On the contrary, as the DNR-e2e (1) algorithm outperforms Node2vec, highest density of the green dots is located on the rightmost part of the triangle.

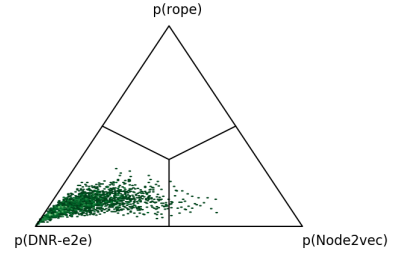
Note that this type of classifier comparison serves as a validation of the critical distance diagrams, and both methods display similar relations between the classifiers.

---

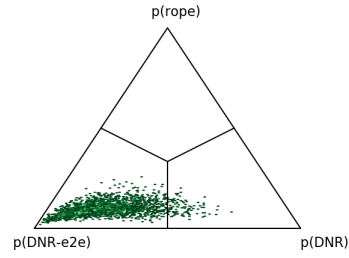
<sup>8</sup> <https://github.com/BayesianTestsML/tutorial/blob/master/Python/Hierarchical%20test.ipynb>



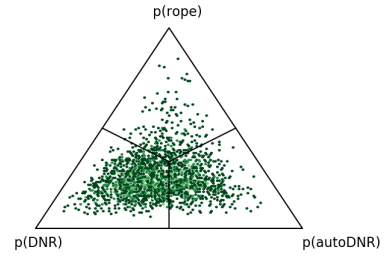
(a) Node2vec (0.465) vs. DNR (0.482)



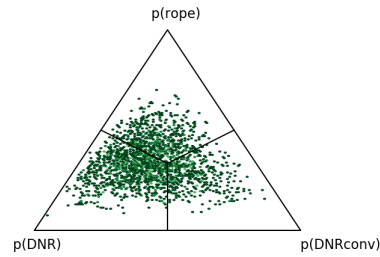
(b) DNR-e2e (0.942) vs. Node2vec (0.051)



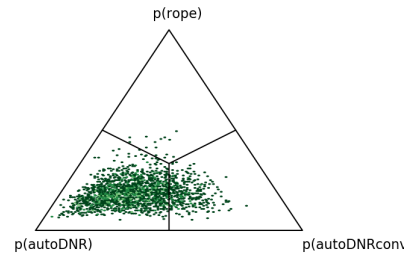
(c) DNR-e2e (0.932) vs. DNR (0.041)



(d) DNR (0.578) vs. autoDNR (0.351)



(e) DNR (0.502) vs. DNRconv (0.192)



(f) autoDNR (0.811) vs. autoDNRconv (0.182)

Fig.9: Pairwise Bayesian performance comparisons of selected classifiers. The probabilities following classifier names represent the probabilities a given classifier outperforms the other.

## 5.2 Time complexity analysis

We present results in terms of running times for node classification in Figure 10.

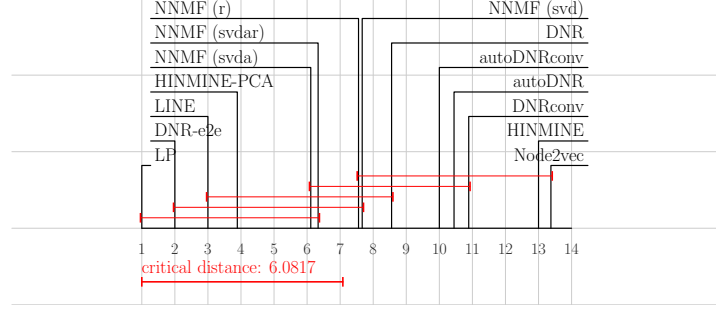


Fig. 10: Average learning and classification time spent over all data sets. Values represent averages over 50 repetitions of the classification task.

The first notable result is fast performance of HINMINE-PCA embeddings. The results suggest, that this approach speeds up the classification compared to the original HINMINE-based classification for more than 10x. The times shown for embedding-based methods are sums of embedding training and logistic regression steps. For example, the  $|N|^2$  matrix of node ranks was for the *Homo sapiens* network obtained in  $\approx 30s$ , yet more than ten times more time was spent on logistic regression. Further, even though e.g., HINMINE-based embedding construction takes on average less than 30 seconds, large portions of its training time are spent at the final class prediction phase.

A similar observation can be made also for node2vec and LINE classifiers. When prediction time is taken into account, the proposed end-to-end family of methods is faster than the embedding-based ones. Even when only network embedding times are considered, the DNR approach are faster than the node2vec approach.

The label propagation algorithm outperforms all the other approaches in terms of time spent both for training and classification. This behavior is expected due to the low time complexity and fast convergence rate of label propagation.

## 5.3 Numerical stability w.r.t. input permutation

One of the non-obvious properties of DNRconv is its (in) dependence with respect to the node order. As we do not employ any information propagation schemes, the node order remains random. To validate the claim that DNRconv performs consistently no matter the order, we conducted 5400 classifications on the Bitcoin

OTC data set using different node orderings and inspected the consistency of the results. We visualize the variability in Figure 11.

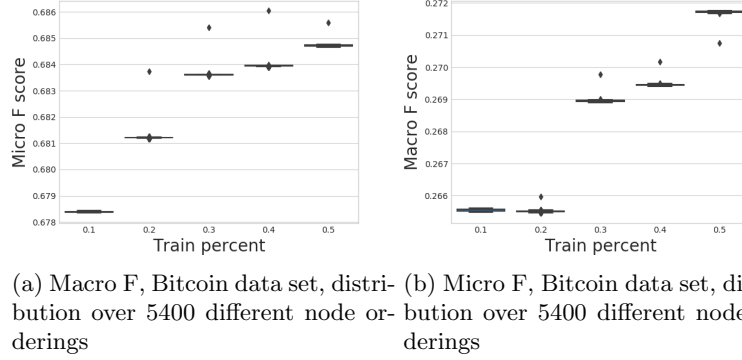


Fig. 11: Numerical stability of the DNRconv embeddings over different node order permutations. Average performance is consistent with respect to train node number (a,b,c,d)

We demonstrate that arbitrary permutations of node orderings yield approximately the same results, hence DNRconv appears robust to input permutation. We believe the reason for such behavior are relatively small convolution regions, followed by average pooling, which unify the node information no matter the input order.

#### 5.4 Qualitative exploration

The main objective of this section was to evaluate how different embedding methods behave out-of-the-box and whether they capture the latent organization of the network in terms of node classes. Unsupervised construction of the network embedding yields potentially interesting representations. We run the embedding methods used with default parameters to construct the embedding of dimension 128 (with the exception of HINMINE, which constructs  $|N|^2$  sized embedding). Next, t-SNE projection [77] is used to reduce the obtained embeddings to two dimensions. Finally, the projections are plotted using Py3plex library [69], where class labels for individual nodes correspond to different colors. The generated visualizations of the Cora network are shown in Figure 12.

We observe the following properties of the obtained visualizations. First, HINMINE-based embeddings appear to encode node information in such a way, that it corresponds well to node class labels. This observation implies that node ranks contain certain information about higher-order organization, as labeled by classes. On the contrary, no distinct separation was observed for LINE and node2vec algorithms. As we tested only out-of-the-box parameterizations, we

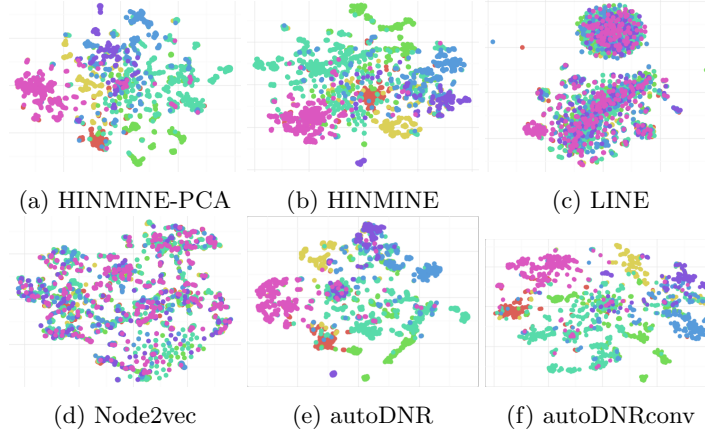


Fig. 12: Visualizations of the Cora network using default t-SNE parameters. Individual classes correspond to different colors. No class information was used to train the embeddings. Each embedding was optimized for 128 dimensions and reduced to two dimensions using t-SNE projections.

believe additional tuning would be needed to produce a better separation or visualization. The produced visualizations of the DNR-based representations show that, DNR, i.e. the shallow architecture successfully groups the classes, yet e.g., green and teal points remain scattered throughout the canvas. Note that the observed visualizations could be the consequence of t-SNE parameterization used. We leave evaluation of this claim for further study, as the goal of this section is to demonstrate DNR indeed clusters the nodes according to class labels.

## 6 Conclusions and Further work

We present a novel DNR approach to complex network node embedding and multilabel node classification. We demonstrate the approach’s scalability and overall performance. The proposed approach is fast and performs better, or comparably well to state-of-the-art approaches. We find that the best-performing DNR variation is a shallow architecture:

$$l_2 = \sigma(w_2(a(w_{\text{dim}}X + b_{l_1})) + b_{l_2});$$

indicating that deeper architectures are possibly not needed for selected tasks. In this setting, the neural network learned the labels in an end-to-end manner.

Our node rank vector computation is designed for parallel or distributed computations, and we believe the DNR is suitable for larger networks (i.e.  $|N| \geq 10^4$ ). Our algorithm for network learning tasks is based on node ranking. We prove empirically, it outperforms current state-of-the-art, even though the network



sampling only leverages first-order random walks—surprisingly, DNR performs comparably to node2vec, which uses information, derived from second-order random walks. We believe this offers opportunity for further improvements with the second- or higher order-random walks in the network sampling part.

We note that Graph convolutional neural networks (GCN) also work well for the problem of end-to-end node classification, especially on block-diagonal adjacency matrix structures [78]. The difference between GCNs and the approach proposed in this work is, that apart from network adjacency matrix and node classes, GCN algorithms require an additional feature matrix, which corresponds to properties of individual nodes. GCNs are thus useful only when features originating from different data sources can be assigned to individual nodes, e.g., the presence of individual words can be assigned as feature vectors to documents representing network's nodes. As P-PR vectors represent features for individual nodes, we see GCN family of algorithms as methods, complementary to the proposed DNR.

One of the unsolved problems in graph deep learning is model interpretability. For example, methods such as node2vec [4] and GCN-like models [78] either construct embeddings by doing local graph crawling, or aggregate the features of close neighbors. The problem which emerges is, importances of individual nodes on the e.g., classifier performance are masked via an embedding layer, or a series of aggregations. Even though a similar problem emerges with the DNR embedding algorithm proposed, the DNR-e2e variation learns directly. This property is for example useful, when a machine learning practitioner wishes to understand exactly which nodes influenced the model's decisions. The recently introduced SHAP algorithm [79], based on coalition theory offers a direct calculation of feature importances, which could be of relevance when the practitioner is attempting to understand the causality behind the learned patterns. We leave evaluation of this idea on more real-world data sets for further work.

The proposed neural network architecture is by no means the optimal solution. We believe that the number of parameters, needed to leverage the network's properties can be reduced significantly whilst maintaining classification performance, yet we leave such exploration for further work. For example, recent improvements in autoML approaches relevant for deep learning topology generation [80] could provide better alternatives.

We next list possible improvements of the DNR:

1. Compared to DNR, the HINMINE methodology can also be used for heterogeneous networks and take into account different relations between nodes. The proposed DNR algorithm is a natural upgrade to the HINMINE methodology and is capable of leveraging properties of heterogeneous networks, which we prove by using the E-commerce data set. We leave more extensive learning tasks on heterogeneous networks for further work.
2. Current DNR implementation is based on the P-PRS vectors, calculated for individual nodes. The input vectors used during learning are thus one dimensional. One could potentially extend individual rank vectors with other node features. The only change to the proposed DNR implementation would thus

include three or more dimensional tensors as inputs, which would represent node features.

3. As current implementation of DNR leverages only first order random walks, we believe its performance could be further improved by using higher-order Markov dynamics. As current state-of-the-art node ranking algorithms can already incorporate such information, the next step for the DNR methodology is also an extension to second and higher order random walks. One possible solution to this problem is the recently introduced Multilinear PageRank [81].
4. The P-PRS with shrinking algorithm used can be implemented on GPUs, which could offer additional speed-ups, especially for larger networks. Finally, we did not consider edge classification tasks, although every embedding can also be used to construct edge representations. We leave such experiment for further work.

We finally discuss some of the experimental attempts which yielded poor performance, yet could be of potential use as a reference for future research.

1. P-PRS vector discretization. We attempted to discretize the P-PRS vectors prior to learning. Here, we experimented with various bin sizes, ranging from 0.01 to 0.0005 — the discretization interval was  $[0, 1]$ . Results were significantly worse compared to using P-PRS vectors directly.
2. Deeper architectures. We experimented with architectures with up to three hidden layers prior to the embedding layer. Performance notably decreased when more layers were added.

**Availability.** The DNR framework is freely accessible at <http://github.com/DNR>. Newly constructed benchmark data sets are available at <http://insilab.org/downloads/> and at the official repository of the algorithm.

**Acknowledgments.** The work of the first author was funded by the Slovenian Research Agency through a young researcher grant (TSP). The work of other authors was supported by the Slovenian Research Agency (ARRS) core research programme *Knowledge Technologies* (P2-0103) and two ARRS funded research projects: *HinLife: Analysis of Heterogeneous Information Networks for Knowledge Discovery in Life Sciences* (J7-7303) and *Semantic Data Mining for Linked Open Data* (financed under the ERC Complementary Scheme, N2-0078). We are grateful to Marko Robnik-Šikonja and to anonymous reviewers for valuable comments and suggestions that helped us to refine the paper. We also gratefully acknowledge the support of NVIDIA Corporation for the donation of Titan-XP GPU used in GPU-based network community detection performed in this work. This research work is supported by Slovenian Research agency (ARRS) project L7-8269—New approaches for better biopharmaceuticals.

## Bibliography

- [1] Benson, A.R., Gleich, D.F., Leskovec, J.: Higher-order organization of complex networks. *Science* **353**(6295) (2016) 163–166
- [2] Nowzari, C., Preciado, V.M., Pappas, G.J.: Analysis and control of epidemics: A survey of spreading processes on complex networks. *IEEE Control Systems* **36**(1) (2016) 26–46
- [3] Le, D.H.: A novel method for identifying disease associated protein complexes based on functional similarity protein complex networks. *Algorithms for Molecular Biology* **10**(1) (2015) 14
- [4] Grover, A., Leskovec, J.: node2vec: Scalable feature learning for networks. In: *Proceedings of the 22nd ACM SIGKDD International Conference on Knowledge Discovery and Data Mining*, San Francisco, California, USA (2016)
- [5] Jilinc, M., Matwin, S., Turcotte, M.: Annotation concept synthesis and enrichment analysis: A logic-based approach to the interpretation of high-throughput experiments. *Bioinformatics* **27**(17) (2011) 2391–2398
- [6] Žitnik, M., Leskovec, J.: Predicting multicellular function through multi-layer tissue networks. *Bioinformatics* **33**(14) (2017) i190–i198
- [7] Perozzi, B., Al-Rfou, R., Skiena, S.: Deepwalk: Online learning of social representations. In: *Proceedings of the 20th ACM SIGKDD international conference on Knowledge discovery and data mining*, ACM (2014) 701–710
- [8] Goodfellow, I., Bengio, Y., Courville, A.: *Deep Learning*. MIT Press (2016) <http://www.deeplearningbook.org>.
- [9] LeCun, Y., Bengio, Y., Hinton, G.: Deep learning. *Nature* **521**(7553) (2015) 436–444
- [10] Krizhevsky, A., Sutskever, I., Hinton, G.E.: Imagenet classification with deep convolutional neural networks. In: *Advances in neural information processing systems*. (2012) 1097–1105
- [11] Wang, D., Cui, P., Zhu, W.: Structural deep network embedding. In: *Proceedings of the 22Nd ACM SIGKDD International Conference on Knowledge Discovery and Data Mining*. KDD '16, New York, NY, USA, ACM (2016) 1225–1234
- [12] Costa, L.d.F., Rodrigues, F.A., Travieso, G., Villas Boas, P.R.: Characterization of complex networks: A survey of measurements. *Advances in physics* **56**(1) (2007) 167–242
- [13] Van Der Hofstad, R.: *Random graphs and complex networks* (2016)
- [14] Wang, X., Cui, P., Wang, J., Pei, J., Zhu, W., Yang, S.: Community preserving network embedding. In: *AAAI*. (2017) 203–209
- [15] Duch, J., Arenas, A.: Community detection in complex networks using extremal optimization. *Physical Review E* **72**(2) (2005) 027104
- [16] Malliaros, F.D., Vazirgiannis, M.: Clustering and community detection in directed networks: A survey. *Physics Reports* **533**(4) (2013) 95–142
- [17] Kuncheva, Z., Montana, G.: Community detection in multiplex networks using locally adaptive random walks. In: *Advances in Social Networks Analysis and Mining (ASONAM)*, 2015 IEEE/ACM International Conference on, IEEE (2015) 1308–1315

- [18] Rosvall, M., Axelsson, D., Bergstrom, C.T.: The map equation. *The European Physical Journal-Special Topics* **178**(1) (2009) 13–23
- [19] Zhu, X., Ghahramani, Z.: Learning from labeled and unlabeled data with label propagation. Technical report (2002)
- [20] Cui, P., Wang, X., Pei, J., Zhu, W.: A survey on network embedding. *IEEE Transactions on Knowledge and Data Engineering* (2018)
- [21] Heimann, M., Koutra, D.: On generalizing neural node embedding methods to multi-network problems. In: *KDD MLG Workshop*. (2017)
- [22] Tang, J., Qu, M., Wang, M., Zhang, M., Yan, J., Mei, Q.: Line: Large-scale information network embedding. In: *Proceedings of the 24th International Conference on World Wide Web, International World Wide Web Conferences Steering Committee* (2015) 1067–1077
- [23] Qiu, J., Dong, Y., Ma, H., Li, J., Wang, K., Tang, J.: Network embedding as matrix factorization: Unifying deepwalk, line, pte, and node2vec. In: *Proceedings of the Eleventh ACM International Conference on Web Search and Data Mining. WSDM '18*, New York, NY, USA, ACM (2018) 459–467
- [24] Goyal, P., Ferrara, E.: Graph embedding techniques, applications, and performance: A survey. *arXiv preprint arXiv:1705.02801* (2017)
- [25] Zoph, B., Le, Q.V.: Neural architecture search with reinforcement learning. *arXiv preprint arXiv:1611.01578* (2016)
- [26] Abadi, M., Barham, P., Chen, J., Chen, Z., Davis, A., Dean, J., Devin, M., Ghemawat, S., Irving, G., Isard, M., et al.: Tensorflow: A system for large-scale machine learning. In: *OSDI. Volume 16*. (2016) 265–283
- [27] Paszke, A., Gross, S., Chintala, S., Chanan, G., Yang, E., DeVito, Z., Lin, Z., Desmaison, A., Antiga, L., Lerer, A.: Automatic differentiation in pytorch. (2017)
- [28] Bastien, F., Lamblin, P., Pascanu, R., Bergstra, J., Goodfellow, I., Bergeron, A., Bouchard, N., Warde-Farley, D., Bengio, Y.: Theano: new features and speed improvements. *arXiv preprint arXiv:1211.5590* (2012)
- [29] Jia, Y., Shelhamer, E., Donahue, J., Karayev, S., Long, J., Girshick, R., Guadarrama, S., Darrell, T.: Caffe: Convolutional architecture for fast feature embedding. In: *Proceedings of the 22nd ACM international conference on Multimedia*, ACM (2014) 675–678
- [30] Rumelhart, D.E., Hinton, G.E., Williams, R.J.: Learning internal representations by error propagation. Technical report, California Univ San Diego La Jolla Inst for Cognitive Science (1985)
- [31] LeCun, Y., Boser, B., Denker, J.S., Henderson, D., Howard, R.E., Hubbard, W., Jackel, L.D.: Backpropagation applied to handwritten zip code recognition. *Neural computation* **1**(4) (1989) 541–551
- [32] Kingma, D.P., Ba, J.: Adam: A method for stochastic optimization. *arXiv preprint arXiv:1412.6980* (2014)
- [33] Srivastava, N., Hinton, G., Krizhevsky, A., Sutskever, I., Salakhutdinov, R.: Dropout: A simple way to prevent neural networks from overfitting. *The Journal of Machine Learning Research* **15**(1) (2014) 1929–1958
- [34] Page, L., Brin, S., Motwani, R., Winograd, T.: The PageRank citation ranking: Bringing order to the web. Technical report, Stanford InfoLab (November 1999)

- [35] Xing, W., Ghorbani, A.: Weighted PageRank algorithm. In: Proceedings of the 2nd Annual Conference on Communication Networks and Services Research, IEEE (2004) 305–314
- [36] Jeh, G., Widom, J.: SimRank: A measure of structural-context similarity. In: Proceedings of the 8th ACM SIGKDD International Conference on Knowledge Discovery and Data Mining, ACM (2002) 538–543
- [37] Kondor, R.I., Lafferty, J.D.: Diffusion kernels on graphs and other discrete input spaces. In: Proceedings of the 19th International Conference on Machine Learning. (2002) 315–322
- [38] Kleinberg, J.M.: Authoritative sources in a hyperlinked environment. *Journal of the ACM* **46**(5) (1999) 604–632
- [39] Crestani, F.: Application of spreading activation techniques in information retrieval. *Artificial Intelligence Review* **11**(6) (December 1997) 453–482
- [40] Zhang, L., Ma, B., Li, G., Huang, Q., Tian, Q.: PL-ranking: A novel ranking method for cross-modal retrieval. In: Proceedings of the 2016 ACM on Multimedia Conference, ACM (2016) 1355–1364
- [41] Nikolakopoulos, A.N., Garofalakis, J.D.: NCDawareRank: A novel ranking method that exploits the decomposable structure of the web. In: Proceedings of the Sixth ACM International Conference on Web Search and Data Mining, ACM (2013) 143–152
- [42] Freeman, L.C.: Centrality in social networks conceptual clarification. *Social Networks* **1**(3) (1979) 215–239
- [43] Freeman, L.C.: A set of measures of centrality based on betweenness. *Sociometry* **40** (1977) 35–41
- [44] Bavelas, A.: Communication patterns in task-oriented groups. *Journal of the Acoustical Society of America* **22** (1950) 725–730
- [45] Katz, L.: A new status index derived from sociometric analysis. *Psychometrika* **18**(1) (1953) 39–43
- [46] Tong, H., Faloutsos, C., Pan, J.Y.: Fast random walk with restart and its applications. In: Proceedings of the Sixth International Conference on Data Mining, Washington, DC, USA (2006) 613–622
- [47] Halu, A., Mondragón, R.J., Panzarasa, P., Bianconi, G.: Multiplex pagerank. *PloS one* **8**(10) (2013) e78293
- [48] Yu, X., Lilburn, T.G., Cai, H., Gu, J., Korkmaz, T., Wang, Y.: Pagerank influence analysis of protein-protein association networks in the malaria parasite plasmodium falciparum. *International Journal of Computational Biology and Drug Design* **10**(2) (2017) 137–156
- [49] Lofgren, P., Banerjee, S., Goel, A.: Bidirectional pagerank estimation: From average-case to worst-case. In: International Workshop on Algorithms and Models for the Web-Graph, Springer (2015) 164–176
- [50] Lofgren, P., Banerjee, S., Goel, A.: Personalized pagerank estimation and search: A bidirectional approach. In: Proceedings of the Ninth ACM International Conference on Web Search and Data Mining, ACM (2016) 163–172
- [51] Kralj, J., Robnik-Šikonja, M., Lavrač, N.: Hinmine: heterogeneous information network mining with information retrieval heuristics. *Journal of Intelligent Information Systems* (2017) 1–33

- [52] Kralj, J., Vavpetič, A., Dumontier, M., Lavrač, N.: Network ranking assisted semantic data mining. In Ortuño, F., Rojas, I., eds.: *Bioinformatics and Biomedical Engineering*, Cham, Springer International Publishing (2016) 752–764
- [53] Page, L., Brin, S., Motwani, R., Winograd, T.: The PageRank citation ranking: Bringing order to the web. Technical report, Stanford InfoLab (November 1999)
- [54] Qiu, J., Dong, Y., Ma, H., Li, J., Wang, K., Tang, J.: Network embedding as matrix factorization: Unifying deepwalk, line, pte, and node2vec. In: *Proceedings of the Eleventh ACM International Conference on Web Search and Data Mining, WSDM '18*, New York, NY, USA, ACM (2018) 459–467
- [55] Shvachko, K., Kuang, H., Radia, S., Chansler, R.: The hadoop distributed file system. In: *2010 IEEE 26th Symposium on Mass Storage Systems and Technologies (MSST)*. (May 2010) 1–10
- [56] Stark, C., Breitkreutz, B.J., Chatr-Aryamontri, A., Boucher, L., Oughtred, R., Livstone, M.S., Nixon, J., Van Auken, K., Wang, X., Shi, X., et al.: The biogrid interaction database: 2011 update. *Nucleic acids research* **39**(suppl.1) (2010) D698–D704
- [57] Mahoney, M.: Large text compression benchmark. URL: <http://www.matmahoney.net/text/text.html> (2011)
- [58] Zafarani, R., Liu, H.: Social computing data repository at asu (2009)
- [59] Stark, C., Breitkreutz, B.J., Reguly, T., Boucher, L., Breitkreutz, A., Tyers, M.: Biogrid: a general repository for interaction datasets. *Nucleic acids research* **34**(suppl.1) (2006) D535–D539
- [60] Lu, Q., Getoor, L.: Link-based classification. In: *Proceedings of the 20th International Conference on Machine Learning (ICML-03)*. (2003) 496–503
- [61] Kumar, S., Spezzano, F., Subrahmanian, V., Faloutsos, C.: Edge weight prediction in weighted signed networks. In: *Data Mining (ICDM), 2016 IEEE 16th International Conference on*, IEEE (2016) 221–230
- [62] Škrlj, B., Kunej, T., Konc, J.: Insights from ion binding site network analysis into evolution and functions of proteins. *Molecular informatics* (2018)
- [63] Konc, J., Janežič, D.: Probis-ligands: a web server for prediction of ligands by examination of protein binding sites. *Nucleic acids research* **42**(W1) (2014) W215–W220
- [64] Konc, J., Depolli, M., Trobec, R., Rozman, K., Janežič, D.: Parallel-probis: Fast parallel algorithm for local structural comparison of protein structures and binding sites. *Journal of computational chemistry* **33**(27) (2012) 2199–2203
- [65] Konc, J., Škrlj, B., Erzen, N., Kunej, T., Janežic, D.: Genprobis: web server for mapping of sequence variants to protein binding sites. *Nucleic acids research* **45**(W1) (2017) W253–W259
- [66] Demšar, J.: Statistical comparisons of classifiers over multiple data sets. *Journal of Machine learning research* **7**(Jan) (2006) 1–30
- [67] Hagberg, A., Swart, P., S Chult, D.: Exploring network structure, dynamics, and function using networkx. Technical report, Los Alamos National Lab.(LANL), Los Alamos, NM (United States) (2008)

- [68] Walt, S.v.d., Colbert, S.C., Varoquaux, G.: The numpy array: a structure for efficient numerical computation. *Computing in Science & Engineering* **13**(2) (2011) 22–30
- [69] Škrlj, B., Kralj, J., Vavpetič, A., Lavrač, N.: Community-based semantic subgroup discovery. In: *International Workshop on New Frontiers in Mining Complex Patterns*, Springer (2017) 182–196
- [70] Jones, E., Oliphant, T., Peterson, P.: *{SciPy}: open source scientific tools for {Python}*. (2014)
- [71] Zhu, X., Ghahramani, Z.: Learning from labeled and unlabeled data with label propagation. (2002)
- [72] Pedregosa, F., Varoquaux, G., Gramfort, A., Michel, V., Thirion, B., Grisel, O., Blondel, M., Prettenhofer, P., Weiss, R., Dubourg, V., et al.: Scikit-learn: Machine learning in python. *Journal of machine learning research* **12**(Oct) (2011) 2825–2830
- [73] Févotte, C., Idier, J.: Algorithms for nonnegative matrix factorization with the  $\beta$ -divergence. *Neural computation* **23**(9) (2011) 2421–2456
- [74] Jolliffe, I.: Principal component analysis. In: *International encyclopedia of statistical science*. Springer (2011) 1094–1096
- [75] Mitliagkas, I., Caramanis, C., Jain, P.: Memory limited, streaming pca. In: *Advances in Neural Information Processing Systems*. (2013) 2886–2894
- [76] Benavoli, A., Corani, G., Demsar, J., Zaffalon, M.: Time for a change: a tutorial for comparing multiple classifiers through Bayesian analysis. *ArXiv e-prints* (June 2016)
- [77] Maaten, L.v.d., Hinton, G.: Visualizing data using t-sne. *Journal of machine learning research* **9**(Nov) (2008) 2579–2605
- [78] Kipf, T.N., Welling, M.: Semi-supervised classification with graph convolutional networks. *arXiv preprint arXiv:1609.02907* (2016)
- [79] Lundberg, S.M., Lee, S.I.: A unified approach to interpreting model predictions. In: Guyon, I., Luxburg, U.V., Bengio, S., Wallach, H., Fergus, R., Vishwanathan, S., Garnett, R., eds.: *Advances in Neural Information Processing Systems* 30. Curran Associates, Inc. (2017) 4765–4774
- [80] Young, S.R., Rose, D.C., Karnowski, T.P., Lim, S.H., Patton, R.M.: Optimizing deep learning hyper-parameters through an evolutionary algorithm. In: *Proceedings of the Workshop on Machine Learning in High-Performance Computing Environments*, ACM (2015) 4
- [81] Gleich, D.F., Lim, L.H., Yu, Y.: Multilinear pagerank. *SIAM Journal on Matrix Analysis and Applications* **36**(4) (2015) 1507–1541

## A Computational complexity of the personalized PageRank with shrinking

The proof of the computational complexity of the P-PRS algorithm used in this work reads as follows:

*Proof.* A naïve PageRank iteration corresponds to multiplying a rank vector with a  $|N|^2$  (dense) matrix. Given this matrix is sparse a single iterations takes up  $\mathcal{O}((|E| + |N|)k)$  time, where  $k$  iterations are needed for convergence with respect to a single node. For all nodes, the complexity is thus  $\mathcal{O}(|N|(|E| + |N|)k)$ .  $\square$

## B Micro and macro overall distributions

Micro and macro distributions over all data sets:

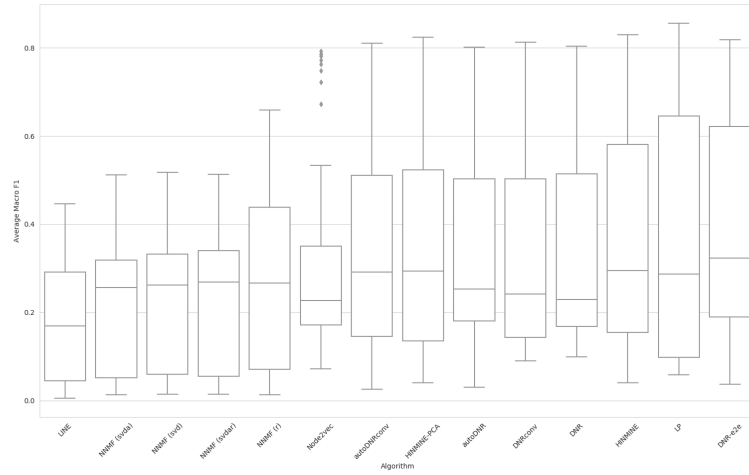


Fig. 13: Overall macro F1 scores averaged over all data sets.



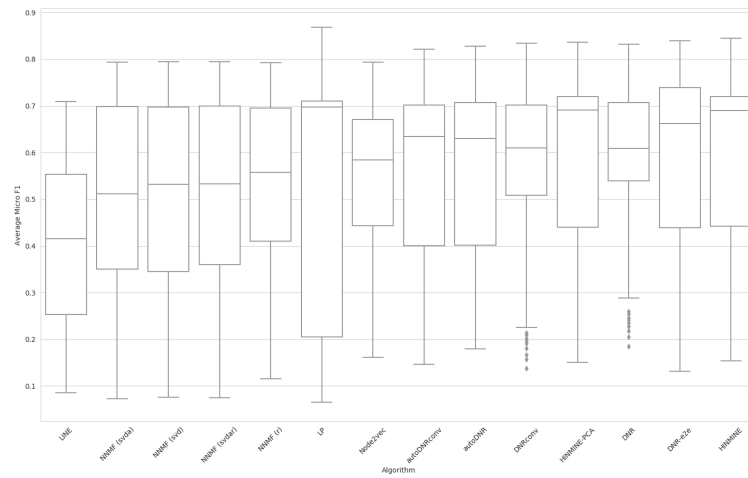


Fig. 14: Overall micro F1 scores averaged over all data sets.

## C Table of results with standard deviations

Numerical results for all scores over 50 runs of the validation procedure:

dataset	Bitcoin	Bitcoin Alpha	Blogspot	CiteSeer	Corra	E-commerce (tf)	Homo Sapiens	PPI	Ions	Wiki
Macro F score										
DNR	0.31 (0.01)	0.22 (0.01)	0.15 (0.01)	0.51 (0.01)	0.78 (0.02)	0.67 (0.0)	0.19 (0.02)	0.22 (0.03)	0.22 (0.03)	0.11 (0.0)
DNR-e2e	0.33 (0.01)	0.31 (0.01)	0.19 (0.02)	0.59 (0.05)	0.79 (0.02)	0.71 (0.01)	0.16 (0.04)	0.34 (0.05)	0.34 (0.05)	0.08 (0.03)
DNRconv	0.31 (0.01)	0.23 (0.01)	0.13 (0.01)	0.49 (0.02)	0.79 (0.02)	0.68 (0.0)	0.16 (0.02)	0.22 (0.03)	0.22 (0.03)	0.1 (0.0)
HINMINE	0.31 (0.01)	0.3 (0.01)	0.12 (0.04)	0.56 (0.04)	0.79 (0.06)	0.67 (0.04)	0.16 (0.04)	0.23 (0.05)	0.23 (0.05)	0.06 (0.01)
HINMINE-PCA	0.31 (0.01)	0.29 (0.01)	0.09 (0.02)	0.51 (0.02)	0.78 (0.05)	0.63 (0.03)	0.15 (0.03)	0.24 (0.04)	0.24 (0.04)	0.07 (0.01)
LINE	0.29 (0.0)	0.29 (0.01)	0.01 (0.0)	0.24 (0.01)	0.4 (0.05)	NaN	0.04 (0.0)	0.12 (0.01)	0.12 (0.01)	0.05 (0.0)
LP	0.29 (0.01)	0.28 (0.01)	0.1 (0.01)	0.61 (0.07)	0.82 (0.0)	0.67 (0.02)	0.07 (0.0)	0.34 (0.03)	0.34 (0.03)	0.06 (0.0)
NNMF (r)	0.28 (0.01)	0.27 (0.01)	0.04 (0.01)	0.47 (0.07)	0.47 (0.17)	0.46 (0.02)	0.1 (0.02)	0.11 (0.03)	0.11 (0.03)	0.04 (0.0)
NNMF (svd)	0.28 (0.01)	0.27 (0.0)	0.04 (0.01)	0.42 (0.09)	0.29 (0.14)	0.47 (0.03)	0.07 (0.03)	0.16 (0.04)	0.16 (0.04)	0.04 (0.0)
NNMF (svda)	0.28 (0.01)	0.28 (0.01)	0.04 (0.01)	0.42 (0.09)	0.32 (0.11)	0.47 (0.03)	0.06 (0.02)	0.15 (0.04)	0.15 (0.04)	0.04 (0.0)
NNMF (svdar)	0.28 (0.01)	0.27 (0.0)	0.04 (0.01)	0.43 (0.09)	0.32 (0.15)	0.47 (0.03)	0.07 (0.03)	0.15 (0.04)	0.15 (0.04)	0.04 (0.0)
Node2vec	0.29 (0.01)	0.22 (0.01)	0.16 (0.02)	0.51 (0.02)	0.76 (0.04)	NaN	0.17 (0.02)	0.28 (0.03)	0.28 (0.03)	0.09 (0.01)
autoDNR	0.31 (0.01)	0.23 (0.01)	0.16 (0.01)	0.49 (0.02)	0.78 (0.02)	0.66 (0.0)	0.19 (0.02)	0.24 (0.03)	0.24 (0.03)	0.04 (0.01)
autoDNRconv	0.3 (0.01)	0.24 (0.02)	0.06 (0.0)	0.49 (0.03)	0.78 (0.03)	0.64 (0.0)	0.16 (0.02)	0.29 (0.03)	0.29 (0.03)	0.03 (0.0)
Micro F score										
DNR	0.71 (0.0)	0.67 (0.01)	0.32 (0.01)	0.56 (0.01)	0.79 (0.01)	0.83 (0.0)	0.23 (0.02)	0.61 (0.04)	0.61 (0.04)	0.55 (0.01)
DNR-e2e	0.67 (0.01)	0.68 (0.01)	0.3 (0.01)	0.62 (0.04)	0.81 (0.02)	0.82 (0.01)	0.19 (0.02)	0.71 (0.05)	0.71 (0.05)	0.46 (0.04)
DNRconv	0.69 (0.01)	0.66 (0.02)	0.28 (0.02)	0.54 (0.02)	0.79 (0.02)	0.83 (0.0)	0.18 (0.03)	0.59 (0.04)	0.59 (0.04)	0.52 (0.01)
HINMINE	0.72 (0.01)	0.71 (0.0)	0.28 (0.04)	0.62 (0.04)	0.8 (0.05)	0.83 (0.01)	0.23 (0.03)	0.68 (0.05)	0.68 (0.05)	0.45 (0.02)
HINMINE-PCA	0.72 (0.01)	0.71 (0.01)	0.25 (0.03)	0.57 (0.02)	0.8 (0.05)	0.82 (0.01)	0.22 (0.03)	0.68 (0.04)	0.68 (0.04)	0.46 (0.02)
LINE	0.69 (0.0)	0.7 (0.01)	0.11 (0.0)	0.33 (0.01)	0.48 (0.03)	NaN	0.09 (0.0)	0.48 (0.01)	0.48 (0.01)	0.41 (0.0)
LP	0.7 (0.01)	0.7 (0.0)	0.21 (0.01)	0.65 (0.06)	0.83 (0.04)	0.72 (0.02)	0.07 (0.0)	0.69 (0.05)	0.69 (0.05)	0.07 (0.0)
NNMF (r)	0.7 (0.01)	0.69 (0.0)	0.16 (0.02)	0.54 (0.06)	0.57 (0.12)	0.78 (0.0)	0.17 (0.03)	0.51 (0.05)	0.51 (0.05)	0.41 (0.0)
NNMF (svd)	0.7 (0.01)	0.7 (0.0)	0.16 (0.02)	0.49 (0.08)	0.45 (0.09)	0.79 (0.01)	0.15 (0.04)	0.6 (0.07)	0.6 (0.07)	0.41 (0.0)
NNMF (svda)	0.7 (0.01)	0.7 (0.0)	0.16 (0.03)	0.49 (0.08)	0.44 (0.07)	0.78 (0.01)	0.13 (0.03)	0.6 (0.07)	0.6 (0.07)	0.41 (0.0)
NNMF (svdar)	0.7 (0.01)	0.7 (0.0)	0.17 (0.02)	0.5 (0.08)	0.46 (0.09)	0.79 (0.01)	0.15 (0.04)	0.59 (0.08)	0.59 (0.08)	0.42 (0.01)
Node2vec	0.67 (0.01)	0.65 (0.01)	0.34 (0.02)	0.56 (0.02)	0.76 (0.03)	NaN	0.2 (0.02)	0.65 (0.04)	0.65 (0.04)	0.51 (0.01)
autoDNR	0.7 (0.01)	0.67 (0.01)	0.32 (0.02)	0.54 (0.02)	0.79 (0.03)	0.83 (0.0)	0.23 (0.02)	0.62 (0.05)	0.62 (0.05)	0.41 (0.01)
autoDNRconv	0.7 (0.01)	0.66 (0.02)	0.2 (0.01)	0.53 (0.04)	0.78 (0.03)	0.82 (0.0)	0.18 (0.02)	0.63 (0.04)	0.63 (0.04)	0.4 (0.0)
Time (s) DNR	145.07 (0.0)	97.1 (0.0)	287.65 (0.0)	84.93 (0.0)	76.15 (0.0)	1010.32 (0.0)	119.2 (0.0)	66.57 (0.0)	66.57 (0.0)	118.04 (0.0)
DNR-e2e	33.46 (13.27)	20.45 (9.1)	83.87 (30.74)	18.42 (8.22)	15.05 (6.51)	511.1 (176.58)	20.73 (9.38)	10.58 (4.47)	10.58 (4.47)	25.61 (11.57)
DNRconv	169.02 (0.0)	121.95 (0.0)	343.42 (0.0)	111.6 (0.0)	95.47 (0.0)	1151.59 (0.0)	157.33 (0.0)	80.8 (0.0)	80.8 (0.0)	141.61 (0.0)
HINMINE	1063.28 (0.0)	411.9 (0.0)	5614.56 (0.0)	117.01 (0.0)	113.79 (0.0)	5560.48 (0.0)	890.23 (0.0)	54.04 (0.0)	54.04 (0.0)	877.45 (0.0)
HINMINE-PCA	57.65 (0.0)	39.19 (0.0)	136.32 (0.0)	33.51 (0.0)	29.72 (0.0)	476.11 (0.0)	57.57 (0.0)	26.79 (0.0)	26.79 (0.0)	55.43 (0.0)
LINE	45.64 (0.0)	37.0 (0.0)	75.02 (0.0)	21.82 (0.0)	21.8 (0.0)	NaN	47.65 (0.0)	21.5 (0.0)	21.5 (0.0)	50.42 (0.0)
LP	0.32 (0.03)	0.22 (0.03)	0.76 (0.02)	0.06 (0.01)	0.06 (0.01)	0.49 (0.01)	1.2 (0.11)	0.09 (0.01)	0.09 (0.01)	0.26 (0.02)
NNMF (r)	132.65 (0.0)	76.17 (0.0)	331.83 (0.0)	51.87 (0.0)	41.05 (0.0)	1295.87 (0.0)	91.64 (0.0)	34.78 (0.0)	34.78 (0.0)	110.63 (0.0)
NNMF (svd)	136.52 (0.0)	75.95 (0.0)	328.9 (0.0)	48.43 (0.0)	51.04 (0.0)	1376.35 (0.0)	89.18 (0.0)	43.53 (0.0)	43.53 (0.0)	112.16 (0.0)
NNMF (svda)	104.83 (0.0)	60.9 (0.0)	331.43 (0.0)	37.12 (0.0)	53.57 (0.0)	782.54 (0.0)	81.2 (0.0)	33.54 (0.0)	33.54 (0.0)	110.98 (0.0)
NNMF (svdar)	121.91 (0.0)	76.13 (0.0)	331.05 (0.0)	49.4 (0.0)	39.51 (0.0)	949.51 (0.0)	76.85 (0.0)	39.2 (0.0)	39.2 (0.0)	110.73 (0.0)
Node2vec	590.61 (0.0)	408.39 (0.0)	1368.54 (0.0)	345.77 (0.0)	301.13 (0.0)	NaN	457.37 (0.0)	239.83 (0.0)	239.83 (0.0)	580.58 (0.0)
autoDNR	160.25 (0.0)	104.16 (0.0)	365.92 (0.0)	91.25 (0.0)	81.88 (0.0)	1356.68 (0.0)	140.04 (0.0)	68.13 (0.0)	68.13 (0.0)	125.31 (0.0)
autoDNRconv	172.36 (0.0)	122.37 (0.0)	277.74 (0.0)	112.22 (0.0)	101.04 (0.0)	1044.71 (0.0)	160.4 (0.0)	83.84 (0.0)	83.84 (0.0)	83.87 (0.0)